Journal of South American Earth Sciences 85 (2018) 168–190

Contents lists available at ScienceDirect

Journal of South American Earth Sciences

journal homepage: www.elsevier.com/locate/jsames

Complex alluvial architecture, paleohydraulics and controls of a multichannel fluvial system: Bajo Barreal Formation (Upper Cretaceous) in the Cerro Ballena anticline, Golfo San Jorge Basin, Patagonia

José Matildo Paredes[a,*], Nicolás Foix[a,b], José Oscar Allard[a], Mauro Nicolás Valle[a,b], Sergio Roberto Giordano[c]

[a] Universidad Nacional de la Patagonia San Juan Bosco, Ruta Nº 1 S/N, Km 4, 9005, Com. Riv., Chubut, Argentina
[b] CONICET (Consejo Nacional de Investigaciones Científicas y Técnicas), Argentina
[c] SINOPEC ARGENTINA Exploration and Production, Inc, Manuela Saenz 323, C1107BPA, Buenos Aires, Argentina

ARTICLE INFO

Keywords:
Alluvial sedimentology
Palaeohydraulics
Outcrop analogs
Humid climate
Upper Cretaceous
Patagonia

ABSTRACT

A sedimentological-architectural review, and a palaeohydrological study was performed in a 380 m thick succession of the Bajo Barreal Formation (Upper Cretaceous) in the Cerro Ballena anticline, Golfo San Jorge Basin, Patagonia. The studied exposure shows, at the base, isolated sandstone channel belts of small scale and low connectivity within siliciclastic floodplain strata (Section A, 185 m thick). It changes upwards into sheet-like, sandstone channel fills with larger interconnectivity that form channel-belt complexes intercalated with thinner floodplain fines of volcaniclastic origin (Section B, 195 m thick). The succession contains seventeen lithofacies and twelve architectural elements that provide information on the alluvial organization of channel and overbank deposits. Palaeoflow data of 218 fluvial channels (Az. 187°; n = 3777) indicate the presence of a depocenter located southward. Seven fluvial styles were identified: 1) multistorey bodies dominated by downstream accretion, 2) multilateral, broad sheets dominated by downstream accretion, 3) narrow sheets dominated by lateral accretion, 4) ribbon or sheet-like bodies infilled by resedimented volcaniclastics, 5) ribbon-shaped fixed channels with attached splays, 6) unconfined, isolated sheet complexes, and 7) unconfined, moderately amalgamated sheet complexes. The variable geometry and style of palaeo-rivers in coeval levels, and dominance of avulsion deposits support that the fluvial system was anabranching, and locally anastomosed. Using palaeohydrological parameters estimated from cross-bed set thickness, a climatic shift toward wetter and more humid climatic conditions from Section A to Section B was demonstrated. We find support to assess the climate as the main external forcing factor on the alluvial organization and stacking density of the Bajo Barreal Formation.

1. Introduction

Ancient fluvial successions display complex internal geometries and architectures, in response to an interplay of extrinsic and intrinsic controls, which in turn controls river plan form, channel-belt dimensions, sediment grain size, and larger scale fluvial architecture. The architecture and evolution of fluvial systems have been of particular interest in both the hydrocarbon industry and academic study in recent years, with detailed investigations using high-resolution 3-D seismic surveys (Posamentier et al., 2007; Ethridge and Schumm, 2007; Reijenstein et al., 2011; El-Mowafy and Marfurt, 2016), modelling studies (Karssenberg et al., 2001; Hajek and Wolinsky, 2012; Keogh et al., 2014) and field-based studies (Labourdette, 2011; Hampson et al., 2013; Allen et al., 2014; Ghinassi et al., 2016, among others). Due to the inability of identify bed-scale stratigraphic features and minor-scale discontinuities using three-dimensional seismic data, the use of analogous systems at outcrops helps to constrain the vertical and lateral variations of sedimentary facies of channel fills, channel-scale stacking styles and stratigraphical relationship with floodplain facies (Pranter and Sommer, 2011; Rittersbacher et al., 2014; Pranter et al., 2014; Paredes et al., 2016).

The Golfo San Jorge Basin, which is located in Central Patagonia, has produced approximately 10 billion barrels of oil (1500 million m^3) during its more than 100 years of development history. With more than 40.000 drilled wells, it currently provides nearly 50% of all liquid hydrocarbons and 13% of all gas of Argentina's production (Secretaría de Energía, 2016). Up to 90% of these hydrocarbons are recovered from fluvial channels in the Upper Cretaceous Bajo Barreal Formation, and

* Corresponding author.
E-mail addresses: paredesj@unpata.edu.ar, paredesjose@yahoo.com (J.M. Paredes).

https://doi.org/10.1016/j.jsames.2018.05.007
Received 6 February 2018; Received in revised form 11 May 2018; Accepted 11 May 2018
Available online 14 May 2018
0895-9811/ © 2018 Elsevier Ltd. All rights reserved.

subsurface equivalents.

The Bajo Barreal Formation at the Cerro Ballena anticline is a well-known outcrop analogue for fluvial reservoirs exposed along a 2500 m width exposure. A previous research identified a lower siliciclastic section with isolated channels at base (Section A, 180 m thick *sensu* Figari et al., 1998) covered by densely-stacked channel belts encased in a fine-grained volcaniclastic floodplain (Section B, 182,5 m thick *sensu* Figari et al., 1998). Although detailed sedimentological data, including qualitative and quantitative information of fluvial sandbodies and floodplain facies were presented by Figari et al. (1998) and Bridge et al. (2000), several questions remain unresolved: Which is the main forcing factor in the upward change of stacking of channelized deposits? How sensitive is the fluvial system to changes in the provision of volcaniclastic particles and, if so, what is the expected fluvial system response?

The general aim of this research is to provide an evaluation of the Bajo Barreal Formation (fluvial, late Cretaceous) in the Cerro Ballena anticline, for identifying spatial and temporal variations in its alluvial organization. The specific objectives of this study are: (1) to analyse the alluvial sedimentology and architecture of the two lithological Sections exposed in the Cerro Ballena area, (2) to quantify the dimensions (true width/thickness) and paleohydrology of fluvial channels or channel belts of both Sections, (3) to unravel the first-order control on the alluvial architecture and stacking patterns. Moreover, the large database of geometries, flow depth and paleohydrological estimations obtained in this research can augment outcrop-analog databases and wire-line log interpretations, and can be useful for researchers working in other hydrocarbon-bearing fluvial successions.

2. Geological setting

The Golfo San Jorge Basin is a continental rift basin broadly E-W oriented, and located in the extra-Andean Patagonia, between 45 and 47°S latitude (Fig. 1A). According to its structural style, the basin was divided (Figari et al., 1999) into five major regions (Fig. 1B). Three of these regions are in the Eastern Sector of the Basin (North Flank, Center of Basin and South Flank), where an extensional style prevails (Figari et al., 1999; Foix et al., 2008). West of this area, is the San Bernardo Fold Belt with an NNW-SSE orientation, which rose up mainly during Neogene times (Peroni et al., 1995; Rodriguez and Littke, 2001). The fifth region, called the Western Sector, is located further west of the Fold Belt and is dominated by extensional structures (Clavijo, 1986), or with little evidence of positive tectonic inversion (Figari et al., 1996; Navarrete et al., 2015).

The Cerro Ballena anticline constitutes the western limb of a faulted, plunging anticline, the axial trace of which is oriented NNW-SSE. Cerro Ballena is bounded to the west by a reverse fault, and to the south by the Deseado River. The strike of the strata is N110°E to N130°E, and dips range from 3° to 50° (Fig. 1C).

The infill of the basin started during the Middle to Late Jurassic, with deposition of a thick succession of basalts, riolites and ignimbrites known as Lonco Trapial or Bahía Laura Group (Lesta and Ferello, 1972), representing the climax of the rift event that led to the fragmentation of Gondwana in southern South America (Fig. 2). A second extensional event took place at the end of the Jurassic and Early Cretaceous, with the conformation of E-W to NNW-SSE striking half-grabens filled by black shales and coastal, wedge-shaped sandstone bodies of lacustrine origin (Figari et al., 1996; Paredes et al., 2018). This stage is represented by strata of the Las Heras Group, only preserved in the subsurface of the basin in isolated depocenters.

The initial Patagonidic tectonic phase (compressional) in the Andean Ranges, located up to 200 kms westward, produced the shifting of the main depocentres of the basin to the Eastern Sector over a regional unconformity and the incorporation of large volumes of fine-grained, ash fall sediments originated in an active volcanic chain along the western margin of Patagonia (Umazano et al., 2009). At the same time, the generation of new WNW-ESE striking normal faults (Uliana et al., 1989; Chelotti, 1997) resulted in the creation of accommodation space for the deposition of the Chubut Group (Barremian to Maastrichtian) in an endorheic basin (Hechem et al., 1990; Hechem and Strelkov, 2002). Initial sedimentation of the Chubut Group occurred in a widely distributed lacustrine unit (Pozo D-129 Formation - Barremian? to Aptian) which was sourced from the north by fluvial systems recorded as the Matasiete Formation (Paredes et al., 2007; Allard et al., 2015). Both units are overlain by the Castillo Formation (Albian), which contains a large proportion of reworked ash-particles in fluvial settings (Umazano et al., 2012; Paredes et al., 2015). The overlying fluvial succession of the Bajo Barreal Formation has been extensively studied since the middle of the past century because of their prolific hydrocarbon production and remaining potential (Feruglio, 1949; Lesta and Ferello, 1972), and due to the occurrence of a diverse continental vertebrate fauna that is among the richest of Patagonian dinosaur-bearing units (Casal et al., 2007; Martínez et al., 2016). Toward the basin margins, the Bajo Barreal Formation is covered by the tuffaceous-loess succession of the Laguna Palacios Formation (Sciutto, 1981) and by Campanian to Maastrichtian fluvial deposits of the Lago Colhué Huapi Formation (Casal et al., 2015).

Covering the Chubut Group, the marine Salamanca Formation (Maastrichtian-early Paleocene) is up to 200 m thick, and it represents the oldest Atlantic transgression in the basin. The overlying fluvial succession of the Río Chico Group is late Paleocene-early Eocene in age. The remaining of the Cenozoic succession is completed with the Sarmiento Formation, EL Huemul Formation, Chenque Formation, Santa Cruz Formation and gravel strata of Plio-Pleistocene age known as “Rodados Tehuelches”.

3. Previous research

The Bajo Barreal Formation (Lesta and Ferello, 1972) and its subsurface equivalents (Lesta, 1968) are distributed over an area exceeding 150.000 km^2, that range from 300 m to up to 2500 m in the Center of Basin (Fitzgerald et al., 1990). Due to its wide distribution in the basin, the unit received varied interpretations, including lacustrine fans, volcaniclastic alluvial fans, meandering and braided rivers in both ephemeral or perennial conditions (Brown et al., 1982; Barcat et al., 1989; Hechem et al., 1990; Legarreta et al., 1993; Rodriguez, 1993; Hechem, 1994, 1997). Along most of the exposures of the San Bernardo fold belt, the Bajo Barreal Formation is divided in two Members: Lower and Upper. The Lower Member is characterized by channelled sandstones interbedded with thicker and finer grained (very fine sand-size) tuffaceous strata, whereas the Upper Member is composed of isolated channel sandbodies surrounded by grey siltstones and siliciclastic mudstones (Figari et al., 1990; Umazano et al., 2008; Paredes et al., 2016). A palynological assemblage recovered from the subsurface of the South Flank (Caleta Olivia Member of the Cañadón Seco Formation = Lower Bajo Barreal Formation) support humid, continental mild to warm climate during Late Albian-Cenomanian times (Archangelsky et al., 1994).

In the area of the Cerro Ballena anticline, Figari et al. (1998) identified three main lithological packages defined according to the occurrence of discontinuities, lithofacies types and stacking patterns, named A, B and C in stratigraphic ascending order. Sections A and B are exposed in the core and western limb of the Cerro Ballena (Fig. 1B) and constitute the main subject of this research, while Section C is partially identified in the southern plunge of the anticline and mainly southward of the Deseado river (Figari et al., 1998). According to Figari et al. (1998) the Section A is a 180 m thick succession of pale green and yellow siltstones interbedded with minor sandstone packages up to 2.5 m thick, interpreted as unconfined sheetfloods and crevasse splays, ephemeral currents and distal mudflows arriving to a low-energy environment with limited paleosoil development. The Section B is a 270 m thick succession that starts at the base of the first level of red-coloured tuffaceous mudstone exposed in the western limb of the Cerro Ballena

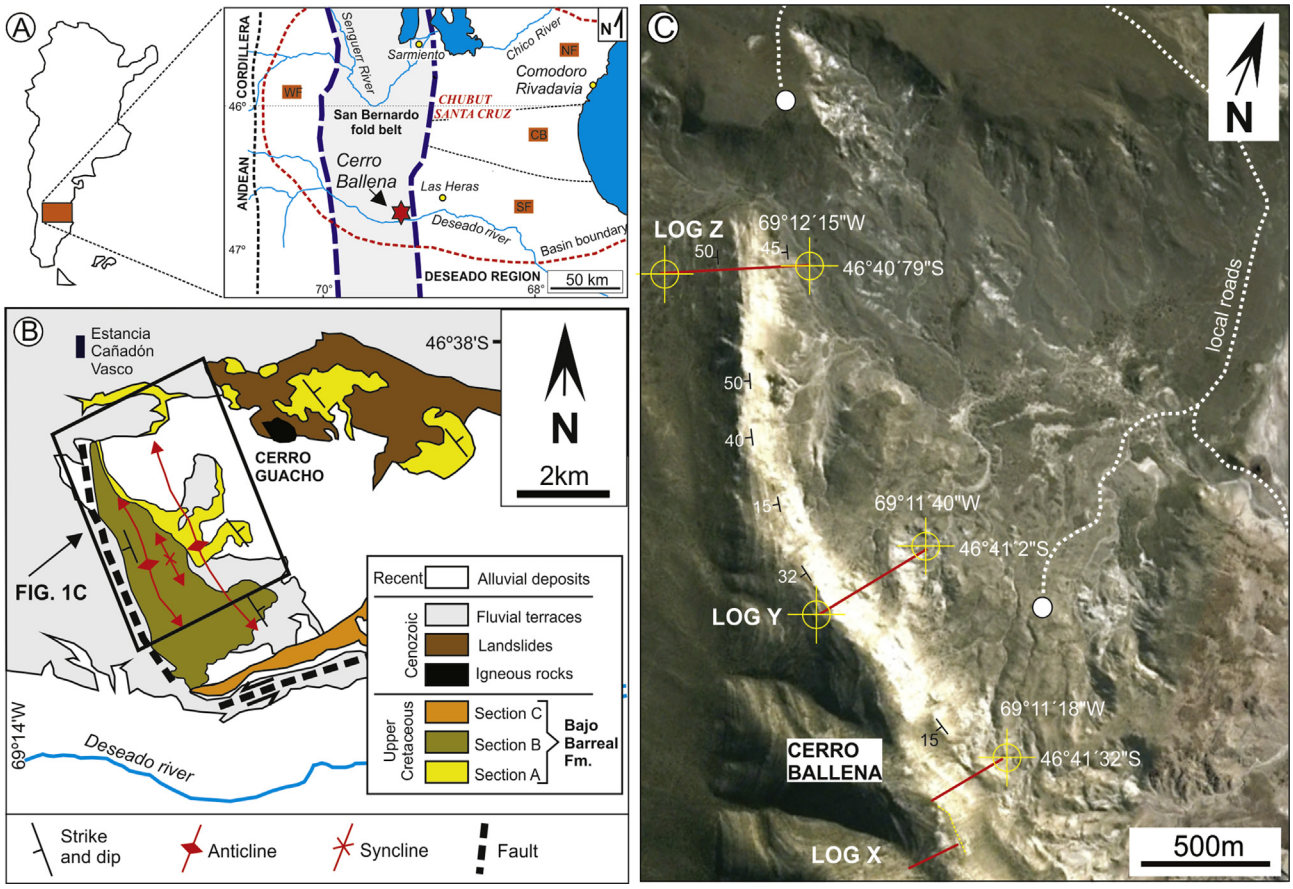

Fig. 1. (A) Location map and structural regions of the Golfo San Jorge Basin, with indication of main localities. Key: SF = South Flank; CB = Center of Basin; NF = North Flank; WF = Western Flank. **(B)** Simplified geological map of the area of the Cerro Ballena anticline, southwestern Golfo San Jorge Basin (after Figari et al., 1998). **(C)** Satellite image of the Cerro Ballena anticline, with location of the position of the sedimentological logs (Logs X, Y and Z). Local roads are indicated as dotted lines. Image from Google Earth.

anticline; it is interpreted as the record of meandering rivers, with well preserved overbank deposits and ocassional provision of ash-fall beds (Figari et al., 1998). The overlying Section C is about 300 m thick and its base is correlatable with the uppermost levels of Section B of the western limb of the anticline. It consists of green to grey mudstones with interbedded sandstones and has been interpreted as sheetflood processes and deposition from distal mudflows in a barreal environment (Figari et al., 1998). Legarreta et al. (1993) have related Sections A, B and C to aggradational, foresteeping and backsteeping system tracts respectively, providing one of the first conceptual models based in field data that relate stacking and geometries of channel belts to base level variations.

Bridge et al. (2000) analyzed the exposures of the Cerro Ballena anticline. They took photos from a helicopter or from adjacent hillslopes and then constructed detailed photomosaics recognizing both the internal geometry and organization of the main channel belts; apparent width and thickness of the sandstones bodies were measured from the tracing (Bridge et al., 2000, p. 341). Several detailed sedimentological logs were carried out at selected accessible locations and in selected channel belts. Bridge et al. (2000) found that the mean thickness of channel sandbodies (n = 117) ranges from decimeters to up to 6 m (mean = 2,09 m), whereas the true widths range from 45 to 274 m (n = 6), and the apparent width/thickness ratio is variable between 17 and 53 (n = 117). Bankfull channel depths ranged from 3 m to 6 m, with reconstructed widths from 35 m to 65 m. Main paleoflow data from the sandbodies is N82°E (n = 97), with most of the values in the range N60°E to N150°E. A radimetrical age of a distinctive marker bed in the base of Section B, interpreted by Bridge et al. (2000) as an ignimbrite, provided an age of 91 ± 0.49 Ma. Most of the fluvial sandbodies were interpreted by Bridge et al. (2000) as single channel rivers of relatively low-sinuosity, with ocassional braided rivers; major spatial changes in sandstone-body proportion and thickness along the exposure were detected. Di Benedetto et al. (2006) imaged channel belts in the nearby Cañadón Vasco oilfield using seismic information, which are mainly W-E oriented at levels of the upper Bajo Barreal Formation, although at deeper levels they are SE and SSE oriented.

4. Methods and terminology

The sedimentary facies of the fluvial succession have been studied by logging at scale 1:50 along well exposed cliff faces. Seventeen lithofacies and twelve architectural elements were described and interpreted. Approximately 3777 paleocurrent measurements, derived from several varieties of cross-bedding, supplement the lithofacies information and aid in the reconstruction of the paleogeographic setting. Paleocurrents were corrected according to the geometrical methods (Ramsay, 1961). The depositional architecture of channel belts has been studied in 2D photomosaics, by measuring local bedding attitude of large-scale inclined surfaces, paleoflow data and dimensions of set thickness of cross-beds. 218 fluvial sandstone bodies were precisely measured (thickness, width) using the Jacob staff and a global positioning system (GPS). To locate stratigraphically all channelized deposits, we measured the floodplain thickness between consecutive fluvial channels, and plotting the extreme coordinates of the sandbodies in a fully 2D scenario. The true width of individual or multi-storey channels were estimated using GPS point data at their margins, and

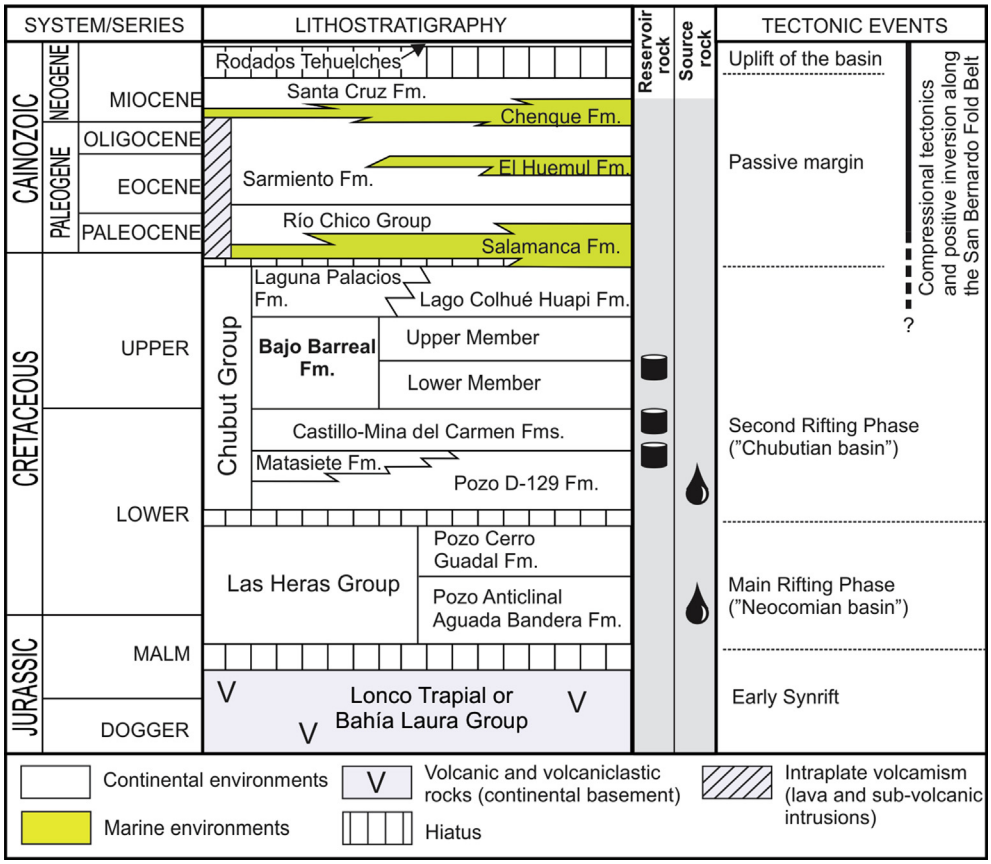

Fig. 2. Stratigraphy and main tectonic events of the Golfo San Jorge Basin, with indication of main source and reservoir rocks. Slightly modified from Paredes et al. (2018).

correcting their apparent width using the mean of the paleocurrent data for each channel. The real width/thickness ratio of fluvial channels (hereafter abbreviated as W:T) was obtained and plotted on frequency histograms and crossplots. Geometry of fluvial channels were classified as ribbons (W:T < 15), narrow sheets (15 > W:T < 100) and broad sheets (W:T > 100) following the Gibling (2006) criteria. Interpretive line drawings of photomosaics of selected multi-storey fluvial channels were used to infer the extent and relationships of stratigraphic surfaces, following a hierarchy of microforms (ripples, laminae), mesoforms (dunes, unit bars), macroforms (compound bars), and channel bodies. Our architectural study follows theoretical or model cross-section diagrams of bars, as those provided by Miall (1985, 1996) and Bridge (1993, 2003), that provide a partial basis for element interpretations.

5. Sedimentology

A study of component facies and alluvial architecture of the Bajo Barreal Formation (Upper Cretaceous) exposed in the core and western limb of the Cerro Ballena anticline has been carried out. In this study, we follow the stratigraphic subdivision of Sections A and B proposed by Figari et al. (1998). The Section A is mainly constituted by mudstones and siltstones, with some channelized sandbodies and scarce participation of tuffaceous strata. It has an overall "mud-sand" ratio of ~6:1, with an upward-increasing sandstone content. The Section B is characterized by the occurrence of fine-grained tuffaceous siltstones, whose chemical alteration and association with fractures produces a distinctive pale red-colour to the succession. Section B contains a distinctive volcaniclastic strata dated in 91 ± 0.49 Ma by Bridge et al. (2000) and a higher proportion of sandstone strata, with an overall "mud-sand" ratio of ~3:1 or larger. The uppermost part of Section B (approx. 80 m thick) was not included in the study due to poor quality of its outcrops.

5.1. Facies

Seventeen lithofacies were defined using lithology, grain size, sedimentary structures, geometries and boundaries. A selected sedimentological log (Log Y) build up during the field study is presented in Fig. 4 to show vertical facies relationships. A summary of main attributes, flow properties and facies interpretation of each facies are presented in Table 1 and selected facies are showed in Fig. 5.

5.2. Architectural elements

The vertical and lateral relationships between the facies in the Cerro Ballena anticline have been used to establish twelve architectural elements. Key distinctive features and detailed interpretations are presented below. For the purpose of clarity, greater detail of channel types and their geometries are presented in later Sections of the paper.

5.2.1. Channel (CH)

Description: The CH element shows flat or erosional base (5th order surface) with concave-up margins to element; the upper surface may be gradational to interbedded mudstones and siltstones. At outcrops, deposits of the CH elements are indurated and resistant to erosion. Individual channel geometries could be found either as isolated sandbodies encased in finer-grained successions or as vertical and lateral stacked sandbodies separated by erosional surfaces. Channel geometries are variable (see section Alluvial organization) with maximum apparent width of 629 m and thickness up to 8.5 m. The CH element consists of any assemblage of Gt or Gm at base, overlied by Sp, St, Sl and Sr facies; it may include SB, LA, DA, HO and ES elements (Fig. 6A). Upward

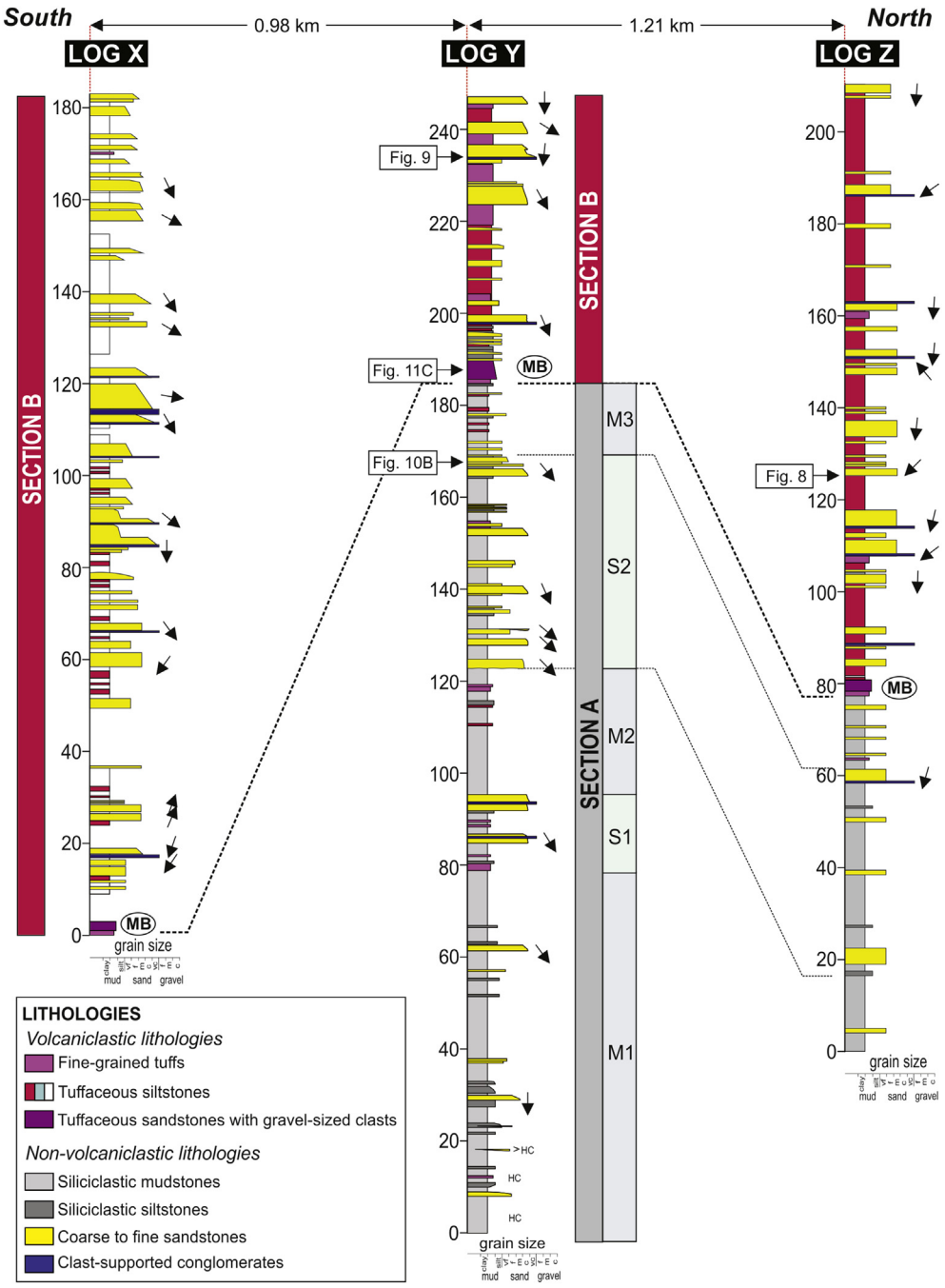

Fig. 3. Lithostratigraphical correlation of the sedimentological sections in the Cerro Ballena anticline. Location of the sedimentary logs is showed in Fig. 1C. MB = Marker bed. The dotted line marks the correlation of the sedimentological sections. Arrows indicate mean paleocurrent vectors (North is up the page). Subdivisions of Section A based in channel occurrence (M1, S1, M2, S2 and M3 in ascending order) are indicated.

fining trend in grain size as well as the preservation of fossil traces occur to the top of the element. Palaeoflow measurements are typically unidirectional and unimodal.

Interpretation: This element is interpreted to represent erosively-based channel element either as single or multistorey channels (Miall, 2014) with geometries variable from narrow ribbon to broad sheets (Gibling, 2006). The deposits were laid down by unidirectional flows in which most of sediment was transported by bedload producing mesoscale and macroscale features (ripples, dunes, bars) indicative of flow regime (see section Composition of channel belts). The fining-upward nature indicate a decrease in flow velocity and suggest a change from bedload to suspended load as the dominant transport mechanism (Fabuel-Perez et al., 2009).

5.2.2. Simple and complex downstream accretion (DA and CDA)

Description: Simple downstream accretion elements (DA) represents the most common architectural element in the study area, being CDA subordinate. They rest on fifth order bounding surface covered by a 25 cm thick, poorly organized, tuffaceous, fine-grained conglomerate (facies Gm) overlied by medium to coarse-grained sandstones containing trough cross bedding (St), low-angle cross bedding (Sla) and plane-parallel lamination (Sl). Foresets are inclined at angles of up to 25°, whereas set bounding surfaces are typically horizontal to inclined at low angle up to 10°. The most examples of CDA are up to 2.3 m thick, and it consists of a similar suite of facies than DA element, with some 0.1–0.3 m thick diffusive gravel layers (facies Gm and Gh) at bases and separated by 3rd order reactivation surfaces (ES element). Some

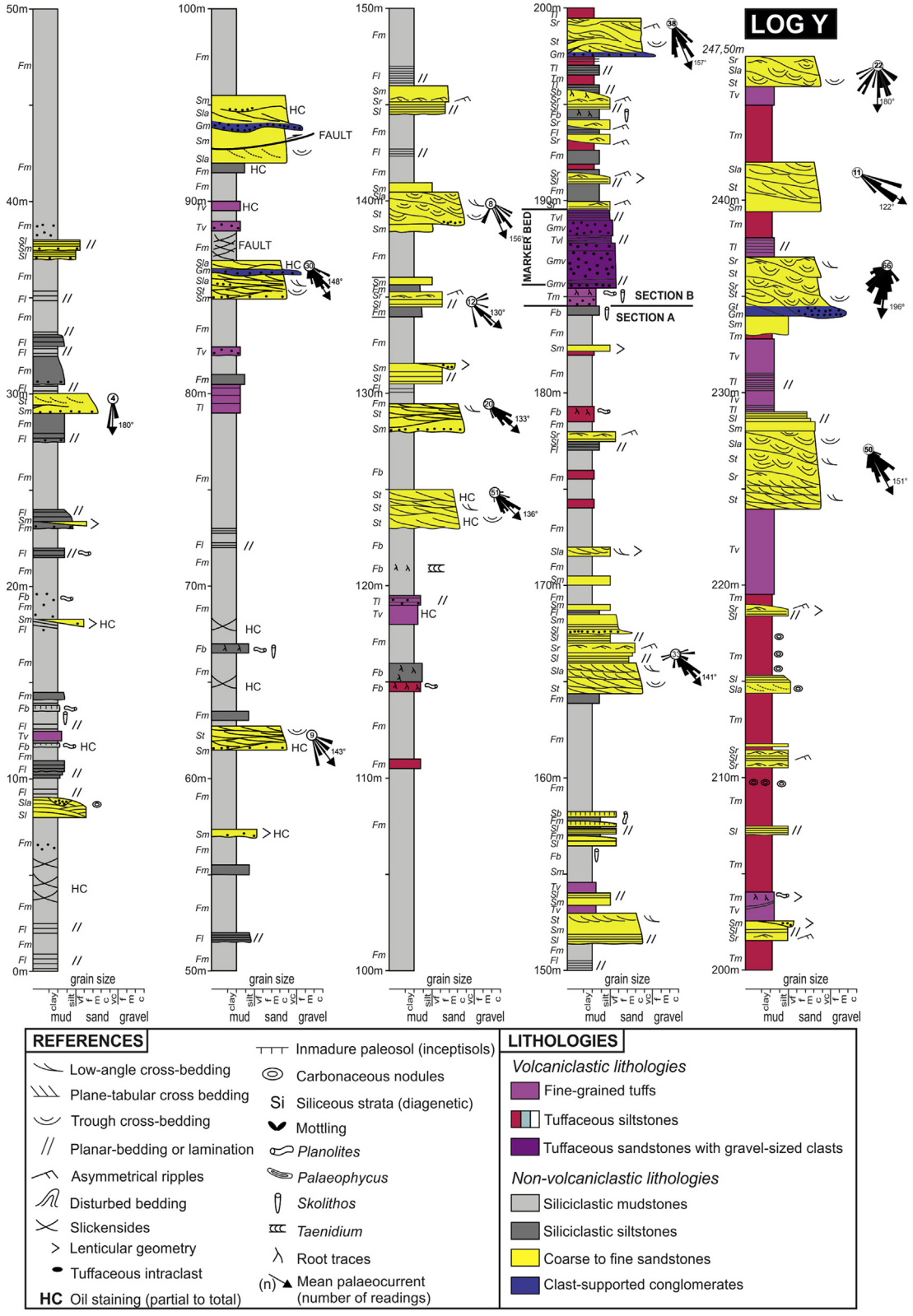

Fig. 4. Composite graphic log (Log Y) of the western limb in Cerro Ballena anticline with palaeocurrent measurements. Location of the section is showed in Fig. 1C.

examples of CDA element show upward decrease in the crossbed set thickness and upward grainsize reduction, with rippled sandstones (facies Sr) and fine-grained tuffaceous sandstones at top, locally with *Skolithos* and *Palaeophycus* ichnogenera.

Interpretation: Most of DA and CDA elements identified were formed by downstream accretion, with uniform paleoflow direction toward the SW being coincident with the dip of accretion surfaces, evidencing bar migration parallel to the main flow direction (Fig. 7B). The upward decrease in set thickness reflects decrease in channel depth through time (cf. Reesink and Bridge, 2007, 2009; Ashworth et al., 2011). Common occurrence of thin gravel layers (Facies Gm) within this element suggest variable discharge during deposition, also

Table 1
Lithofacies of the Bajo Barreal Formation in Cerro Ballena anticline.

Code	Facies and Description	Interpretation
Gmv	*Massive, matrix supported tuffaceous conglomeratate.* Uncommon. Individual beds are up to 1 m thick, have planar and locally erosive base, sheet-like geometry and bimodal grainsize. The matrix consists of coarse to medium-grained tuffaceous sandstones, and contain outsized clasts up to 10 cm in size. Ungraded throughout the bed or coarse-tail normally graded at upper part.	Volcaniclastic debris flow/mudflow. Bulking from initial turbulent flow and rapid deposition from suspension.
Gm	*Massive, clast-supported tuffaceous conglomerate.* Common occurrence. Poorly-sorted, granule to small pebble tuffaceous conglomerate. Diffuse, horizontal stratification.	Fluvial channel lag.
Gt	*Through cross-bedded tuffaceous conglomerate.* Abundant. Tuffaceous, fine-grained conglomerates with clast or matrix supported texture. Crudely bedded or with trough cross-bedding. Matrix of coarse to medium-grained tuffaceous sandstones. Mean size up to 0.5 cm, with rounded clasts up to 7 cm in diameter.	Downstream migration of bars or migration of 3D dunes inside channels.
Sla	*Low-angle cross bedded sandstone.* Abundant. Slightly erosive base, moderate grain size sorting, occasionally with fining upward trend from coarse to fine-grained sandstones. Sets are < 0.5 m thick and 1–4 m of lateral extent. Foresets dip less than 10°. Individual laminae show plane-parallel lamination. Interbedded with massive or trough cross-bedded strata. Trunk remains. Occasional convolute bedding.	Downstream accretion of low relief bedforms with high wavelength/amplitude ratio.
St and Sp	*Trough (St) and planar (Sp) cross-bedded sandstone.* St common, Sp subordinate. Very coarse-grained to fine-grained, sub-angular to sub-rounded sandstone clasts showing moderate sorting. Beds average 0.3–0.6 m thick, with bedsets up to 2 m. Could contain trunk remains or broken dinosaur bones.	Migration of straight-crested (Sp) or curved-crested (St) bedforms in lower flow regime conditions.
Sl	*Parallel-laminated sandstone.* Abundant. Medium to very-fine grained sandstones, with planar base and moderate sorting, occasional outsized clasts. Laminae are few mm to 1 cm in thick and show normal grading. Laminae boundaries defined by changes in the grain size. Frequently interbedded with low-angle cross bedding and/or massive sandstones. Locally convolute lamination chaotically folded.	Deposition under upper-flow regime within a fluvial channel, or as an unconfined fluvial sheetflood.
Sb	*Burrowed sandstone.* Common. Medium to fine-grained sandstones with gradational base to other coarse-grained facies. Contain root traces, mottling and several fossil traces, including *Skolithos*, *Planolites*, and *Taenidium*.	Destruction of depositional structure due to bioturbation.
Sm	*Massive sandstone*. Subordinate. Very coarse to very fine-grained, ungraded, structureless sandstones. Strata are tens of cm thick, with scours at bases. Interbedded with plane-laminated or trough cross-bedded stata.	Rapid deposition of bedload from a highly concentrated sediment during high-discharge conditions.
Sr	*Current-ripple laminated sandstone.* Abundant. Very-fine to fine-grained sandstones with good sorting. Associated to several current-dominated sandstone facies or interbedded with fine-grained, massive tuffaceous sediments. Strata are less than 20 cm in thickness. Unimodal palaeocurrents.	Migration of small bedforms within a fluvial channel or via unconfined flows under lower flow regimes.
Fm and Fl	*Massive (Fm) or horizontally laminated (Fl) siltstone/mudstone.* Abundant in the Section A. Pale-grey siltstone with lower amount of mudstone. Where preserved, laminations are less than 5 mm thick. Frequent incorporation of isolated, tuffaceous clast until 1 cm in diameter, unorganized wood (carbonaceous) fragments. Could contain slickensides.	Settling from suspension within a fluvial channel or in a floodplain environment.
Fb and Tb	*Burrowed mudstone (Fb) or Burrowed tuffaceous siltstone (Tb).* Uncommon. Strata few cm to tens of centimeter thick with motting, *Skolithos* and unidentified fossil traces.	Intense bioturbation of a fine-grained substrate prior to burial.
Tm and Tl	*Massive (Tm) or horizontally laminated (Tl), fine-grained tuffaceous sediment.* Abundant in the Section B, rare in the Section A. Laminae are few mm thick and commonly ungraded, but can be normally graded and contain clasts of coarse tuffaceous sandstones, or pumice fragments up to 1 cm in diameter. Packages can reach up to 10 m of thickness. Contain root traces, intense mottling and several fossil traces, including *Planolites*, and *Palaeophycus* sp. Some beds contain symmetrical ripples and wood fragments on bedding surfaces.	Reworking of pyroclastic sediments by aqueous flows. Later pedogenesis of reworked tuffs.
Tv	*Vitric tuffs.* Subordinate. Strata with planar base and mantle bedding, thickness from few cm to several tens of cm. Could contain pumice outsized clasts interbedded and inverse grading. Biotite grains oriented parallel lo the laminae are common.	Setting of suspended ash in standing water.

indicated by the presence of fossil traces underlying internal bounding surfaces.

5.2.3. Lateral accretion (LA)

Description: The LA element consists of alternated large-scale inclined, coarse-grained cross-stratified (St) to parallel-laminated sandstones (Sl) with gravel layers of about 0.5 m thick (Gm) at base, with ripple-laminated sandstones (Sr) to the top. Lenticular sets of strata formed by accretion of laterally-superposed medium to fine-grained sandstone dip at angles up to 15°, have a convex-upward shape and are separated by erosional surfaces at a lower angle. Three to five laterally accreted packages shift laterally with slight vertical offset; individual convex-upward packages are about 15–20 m wide and up to 2.5 m thick, each separated by massive, fine-grained sandstones (Sm). The dip direction of the accreted surfaces is oriented at high-angle (> 60°) to the paleoflow direction measured on trough cross-bedded units that overlie the large-scale inclined surface (Fig. 6C).

Interpretation: The accretion of lenticular sets dipping at high-angle in relation to paleoflow data of associated channel fills suggest lateral accretion and, therefore, can be interpreted as point bars or bench deposits associated with helicoidal flows (Allen, 1970; Bridge, 1977). Variable paleocurrent directions between superimposed stories indicate sinuous channel systems. The mud drapes on some bedding surfaces may be associated with major floods or seasonal discharge fluctuations. In terms of abundance, LA element has been identified in only 11 channels (about 5% of the analized channel population), being under-represented in relation to DA-CDA elements.

5.2.4. Sandy bedforms (SB)

Description: There is a common architectural element in the study area. Comprise tabular sheets to broadly lenticular bodies of fine-grained to pebbly coarse-grained, St-dominated sandstones overlying - and interbedded with - medium to fine-grained Sr-dominated sandstones. They range from 0.5 to 2 m thick, with uncommon examples as thick as 3 m. Locally could contain convolute lamination commonly flanked by rotated, deformed St foresets (Fig. 6D). Angular to sub-angular intraclasts, 0.5–4.0 cm long, of pale grey tuffaceous sandstones, and thinly laminated, very fine-grained sandstone are commonly present at bedform bases and in their lower parts. In several channels of Section B, the architectural element is dominated by Sr facies

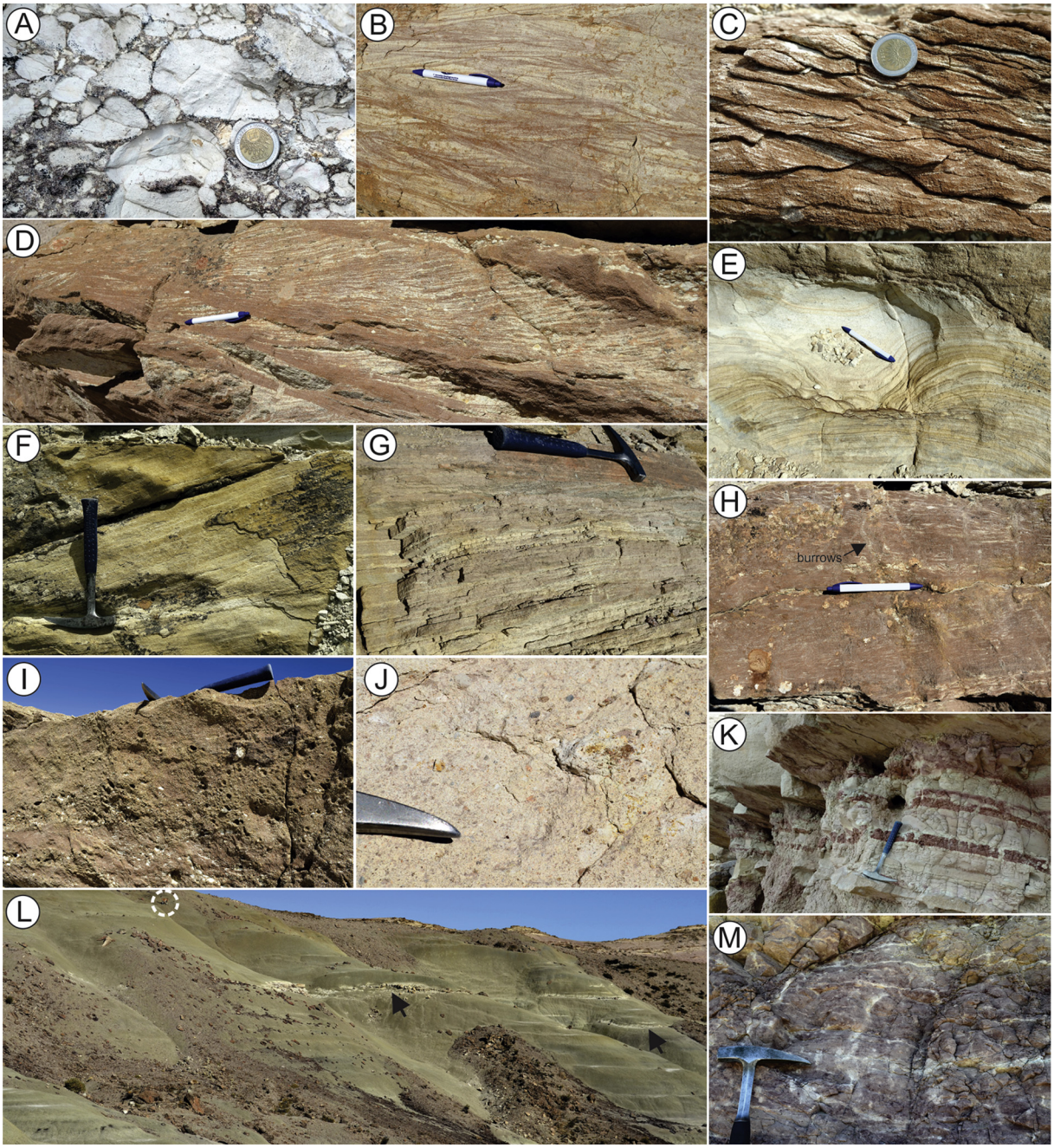

Fig. 5. Typical appearance of facies identified in the Cerro Ballena anticline. **(A)** Clast-supported, fine conglomerate (Facies Gm) at base of a fluvial channel. The dark colour of the matrix is due to hydrocarbon impregnation. Coin is 13 mm in diameter. **(B)** Medium-grained sandstones with low-angle cross-bedding (Facies Sla). Cross-bedded sets are between 8 and 13 cm in height. Pen is 13 cm long. **(C)** Medium to fine-grained sandstones with current ripples (Facies Sr). Coin is 13 mm in diameter. **(D)** Overimposed sets of medium-grained, trough cross-bedded sandstones (Facies St). Pen is 13 cm long. **(E)** Medium to fine-grained sandstones with convolute lamination (Facies Sl). Pen is 13 cm long. **(F)** Coarse to medium-grained sandstones with planar cross bedding (Facies Sp). Sets dip 25–27°. Hammer is 30 cm long. **(G)** Parallel-laminated, medium to fine-grained sandstones (Facies Sl). Hammer is 30 cm long. **(H)** Fine-grained, rippled sandstones (Facies Sr) at the base with fine-grained sandstones displaying meniscate burrows at the top (Facies Sb). Pen is 13 cm long. **(I)** Poorly-organized, massive sandstones with isolated gravel-sized tuffaceous clasts (Facies Sm). Hammer is 30 cm long. **(J)** Details of grain distribution of the massive, lapilli-sized, tuffaceous conglomerate of the marker bed (Facies Gmv). The visible part of the hammer is 7 cm long. **(K)**. Horizontally laminated interbedded tuffaceous siltstones and mudstones (Fl) underlying channel sandstones. Hammer is 30 cm long. **(L)** Typical aspect of grey mudstones in Section A (Fm and Fl facies) and isolated channel belts (arrow). A 1,8 m tall *guanaco* (encircled) for scale. **(M)** Red-coloured tuffaceous siltstones of Section B (Facies Tl). The visible part of the hammer is 25 cm long. (For interpretation of the references to colour in this figure legend, the reader is referred to the Web version of this article.)

throughout most of the preserved thickness. Grain size of this element varies significantly in a vertical section, but individual elements are moderately well sorted, such that some are composed of fine-to medium-grained sandstone, whereas others are pebbly.

Interpretation: Sandy bedforms are deposits of dunes or possibly small bars in broad, low-sinuosity channels (Sambrook Smith et al., 2016), with widths of few tens of meters and typical bankfull depths of at least 4 m, but in some cases the channels were up to 5 m deep. SB elements dominated by Sr facies represent a distinctive pattern of low-energy conditions during the infilling of the channel, probably

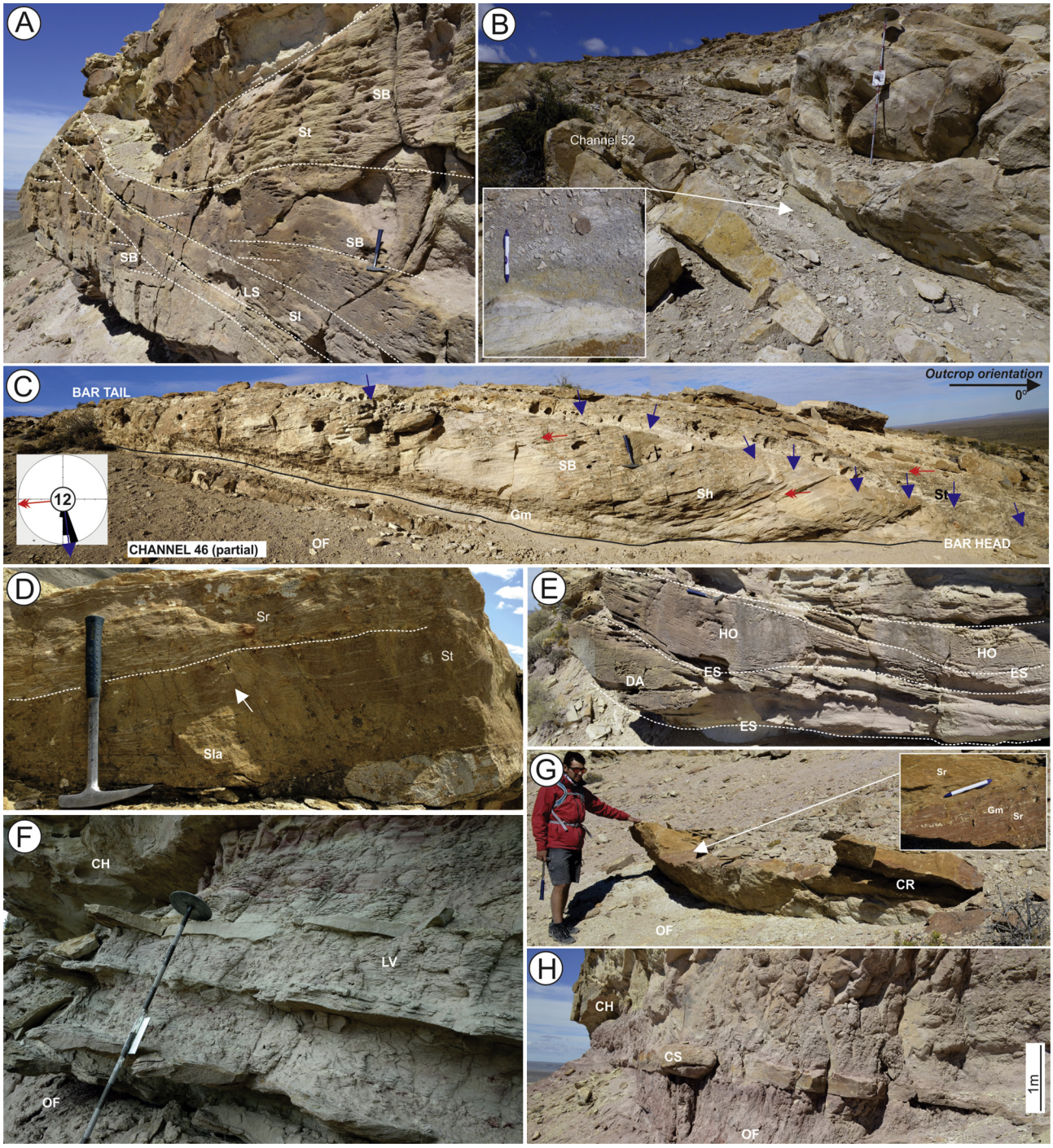

Fig. 6. Examples of architectural elements within the Bajo Barreal Formation at Cerro Ballena anticline. **(A)** Large-scale compound bars in a vertical cliff of Section B. Superposition of accretional units (DA?/LA? elements) up to 2.5 m thick is oblique to the outcrop orientation. Directions of bar accretion and paleoflow are unknown. Hammer is 30 cm long. **(B)** Grey mudstones infilling Channel 52, representing abandonment (FFC element) of the channel. The Jacob's staff is 1.50 m long. **(C)** Solitary unit bar in Channel 46, Section B. The outcrop is oriented parallel to the paleoflow. Note the lobate top and relatively simple internal arrangement of accretion units. The unit bar is overlain by cross-bedded sandstones with paleocurrent data at high angle in relation to accretion surfaces. Hammer is 30 cm long. **(D)** Sandy bedforms (SB element) composed by Sla, St and Sr facies. The white arrow indicates locally deformed (convolute bedding) strata. Hammer is 30 cm long. **(E)** Hollow element (HO). Superposition of sandy strata with concave-upward, scoop-shaped scours (ES element) infilled by accretionary, plane-parallel laminations (Sl facies). Hammer is 30 cm long. **(F)** Alternation of sandstone lenses and plane-parallel laminated siltstones preserved in levee deposits (LV element). Each division of the Jacob staff is 10 cm long. **(G)** Small-scale crevasse channel (CR element) with evidences of oblique infilling during alternating phases of high and low-energy flow conditions. Person is 175 cm tall. **(H)** Proximal floodplain deposits of the Section B. Lobate sandstone deposits (CS element) interbedded with reddish tuffaceous siltstones (OF element). Code of facies is in Table 1.

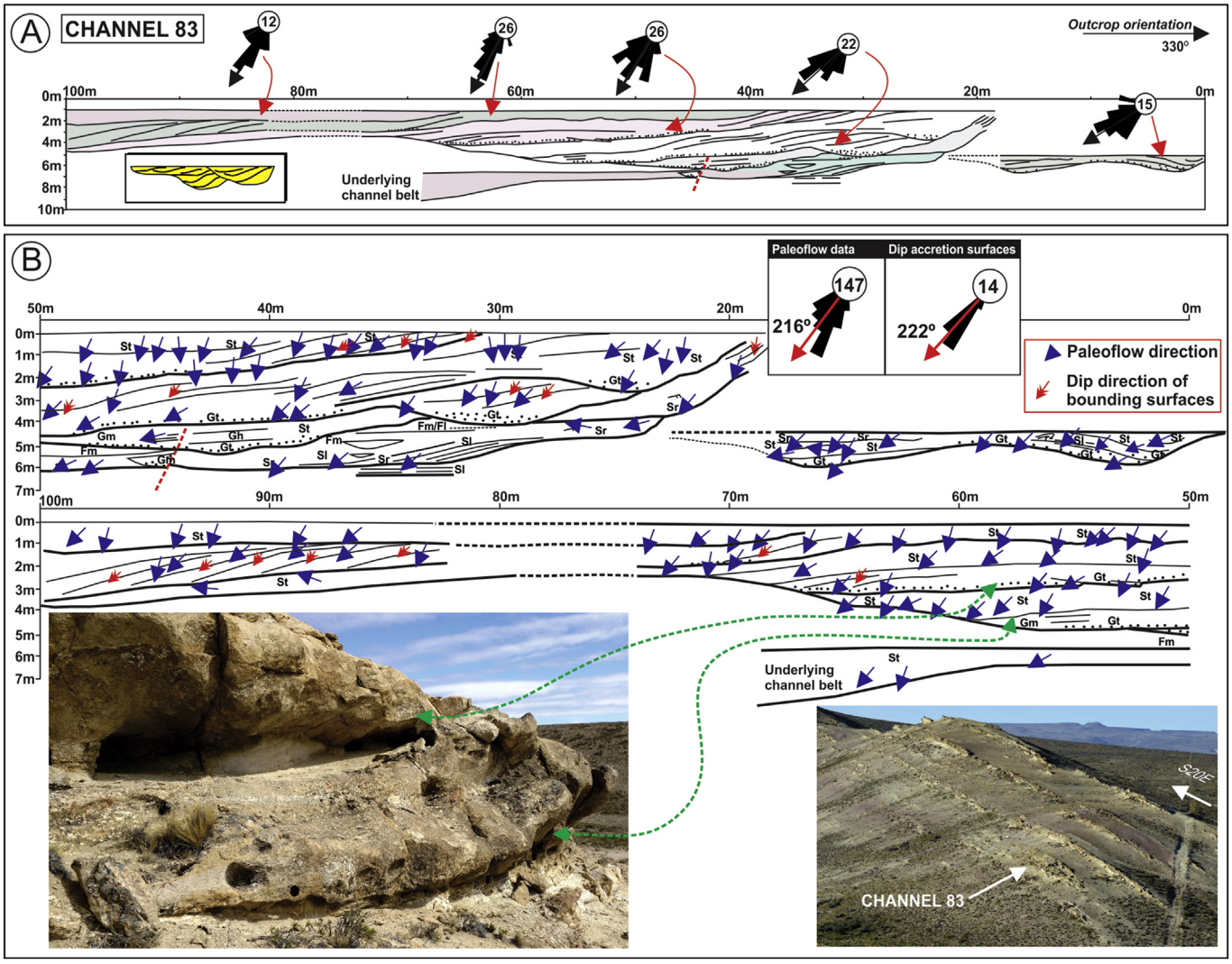

Fig. 7. Alluvial architecture style 1: Multistorey, low-sinuosity channel belts dominated by downstream accretion (DA element). The upper panel (A) contains information of the main stories identified in the channel belt, with averaged paleocurrent values for each story. The inset shows a summary diagram with the main attributes. The lower panel (B) exhibits details of bedding characteristics, paleoflow data and dips of accretion surfaces. For these vectors, the north is up to the page. Note in the box that paleoflow data and dips of accretion surfaces are roughly parallel, evidencing downstream migration of macroforms. Code of facies and architectural elements is in Table 1. Channel 83 belong to Section B, at the northernmost part of the study area.

associated to a partially abandoned channel or to a secondary channel located adjacent of a main channel, infilled mainly during overbank floods.

5.2.5. Laminated sheet sandstones (LS)

Description: The LS element has sheet-like geometry and fining-upward grainsize, overlying a flat to low-relief erosion surface. This element is characterized by laminated sandstones (Sl facies) in association with sandstones containing current ripples (Sr) and low-angle cross-bedding (Sla), although a few examples evidence lateral gradation to massive, medium-grained sandstones (Sm). Typical thickness ranges from 0.3 to 0.6 m, with few meters to tens of meters of apparent width.

Interpretation: Plane-parallel sandstone deposition is interpreted in terms of transportation in upper flow regime conditions in very shallow water depths (Alexander and Fielding, 1997) during which the sediment aggraded vertically (North and Taylor, 1996). In modern rivers, upper flow regime bedforms are preserved mainly due to very rapid changes in the flow stage, such that there is insufficient time during falling stage for the stream bed to re-equilibrate and rework those bedforms into lower flow regime bedforms (cf. Jones, 1977). Since the preservation of upper flow regime conditions is favoured under hydrological conditions characterized by abrupt drops in flow stage, it seems that abundant preservation of this element may have paleoclimatic significance, pointing to a climatic regime in which a pronounced seasonal maximum in precipitation and runoff occurred (Fielding, 2006).

5.2.6. Erosional scour fill (ES)

Description: The ES element consists of discontinuous sandbodies within concave-upward erosional scours (Fig. 6E) situated in channel fills (CH element). The irregular surface is covered with a lag of tuffaceous intraclasts capped by Gm, St, Sl or Sr facies.

Interpretation: The element represents scour fills developed on channel floor, and over tops and flanks of bars (Miall, 1996).

5.2.7. Hollow element (HO)

Description: The HO elements is characterized by a curved base lacking a flat floor, and a fill composed of a single coset of Sl dipping at an oblique angle to the margin of the hollow. The scoop-shaped sandbodie show a lenticular geometry (Fig. 6E) and reach a few tens of centimetres thick and up to 4 m of lateral extent.

Interpretation: The hollow element represents the rapid cut and fill

of scour hollows at channel confluences downstream from bars or junctions with tributaries (Cowan, 1991; Bristow, 1993).

5.2.8. Abandoned channel (FFC)

Description: This element has been identified in eleven examples of Section B. It is composed of lenticular tuffaceous siltstones (Tm and Tl facies) and very fine-grained, structureless sandstones (Sm) with an overall fining-upward trend, commonly with intraclast mudstone breccias. Fine-grained packages are 1.2–3.5 m thick and 5–25 m width, overlying typical sandy channel (CH) facies (Fig. 6B).

Interpretation: Silty sediments and fine-grained sands were deposited mainly from suspension during waning flow or from repeated flooding as mud plugs (Miall, 1996). This can occur over a long period by sediments from overbank flooding from adjacent active channels, or from more distant sources.

5.2.9. Crevasse channels (CR)

The CR elements are small-scale channel forms with apparent width between 2 and 15 m and maximum thickness from 0.4 to 1 m. The constituent lithofacies are poorly organized granule to pebble conglomerates (Gm facies) at bases, low-angle cross-bedded sandstones (Sla), rippled sandstones (Sr) and laminated sandstones (Sl) toward the top of the element, which could show a fining-upward trend.

Interpretation: Based in the small scale of their features, minor channelized sandbodies are interpreted as crevasse channels cut into the margins of larger channels during high-discharge flood events (Miall, 1996). Fining-upward trends are attributed either to gradual reduction of discharge or to an increase of the distance to active channel belts.

5.2.10. Crevasse splay (CS)

Description: This element, relatively common in Section B, consists of sheet-like, laterally extensive sandstones that exhibit flat, sharp or locally erosive base and convex-upward top. They are 0.5–1.0 m thick and can reach a maximum of 130 m of apparent width. They are composed by horizontally laminated sandstones (Sl), current-ripple cross-laminated sandstones (Sr) and minor massive sandstones (Sm). Other lithofacies included in this element (Sla, St) are rarely observed, constituting ~ 10% of the analyzed examples. The CS element has diffuse gravelly layers (< 0.1 m thick, < 1 m of width) across the strata, and fining-upward grainsize trend. It is relatively common the presence of fossil traces in the top of deposits, which could show gradual thickness variations. Averaged paleocurrents are variable in relation to the adjacent channel fills. Although common in the study succession, as laminated sheet sandstones are much thinner that channelized fluvial sandbodies, they are difficult to distinguish in poorly-exposed sections or may be hidden beneath talus, probably being under-represented in the measured sections.

Interpretation: The sheet-like and lenticular geometry, small thickness, and predominance of structures generated by unidirectional currents in the sandstones and siltstones, combined with their positioning adjacent to - and extending from - channelized fluvial sandbodies (CH), is suggestive of deposition in crevasse splays that formed in response to breaching of a main channel during periods of intermittent overbank flooding (Fielding, 1986). Erosional bases overlain by tuffaceous intraclast deposits (lithofacies Gm) located at the base suggest scouring of a cohesive mudstone substrate by turbulent, unconfined flows during crevasse flooding (Shultz, 1984). The occurrence of pedogenic mottling at multiple bed tops in this arquitectural element suggests repeated periods of nondeposition, and fluctuations in water level and/or episodic deposition on elevated parts of the floodplain (cf. Fielding, 1986; Melvin, 1987).

5.2.11. Levee (LV) element

Description: Levees are not commonly preserved, although it could be due to poorly exposed facies below most of the channel element (CH). It consists of sheet-like to lenticular bodies 30–70 m long and 1–5 m thick, thinning away from a channel margin (Figs. 6F and 5K). They consist of interbedded St, Sr and Sm beds with fine-grained components (OF), commonly associated with CS and CH elements. They appear in few cases as complex patterns of interbedded sandy and tuffaceous siltstones, that may exhibit an overall coarsening-upward trend. The interbedded units are laterally traceable from channel (CH) elements forming “wings”, thinning away from the channel-margin.

Interpretation: Wedge-shaped sandbodies (“wings” sensu Friend, 1983) connected with major channels have been often interpreted as natural levee deposits (Kraus, 1996; Miall, 1996; Jo, 2003).

5.2.12. Overbank fines (OF)

Description: This element makes up much of the Bajo Barreal Formation at Cerro Ballena. Both siliciclastic mudstones and tuffaceous siltstones are rarely plane-laminated; more commonly, especially toward the top of unit, they are strongly mottled. It consists of mudstone blankets, massive (Fm, Tm) or laminated (Fl, Tl) fine-grained beds, with or without minor sandstone lenses and/or sandstone load structures. Ocassional fine-ash strata (Tv) tens of centimeters thick can be found.

Interpretation: Sedimentation may have taken place from suspension settling from unconfined flows during repeated minor flood events, or likely in temporary lakes on the floodplain (Umazano et al., 2008). The rare presence of lamination indicates deposition from suspension. Paleosols are weakly developed and lack of distinctive horizons.

5.3. Composition of channel belts

The basic unit of external architecture construction in a fluvial succession is the channel belt (Gibling, 2006). Five architectural styles were established for channel belts (Styles 1–5) based in the identification of morphological features (e.g. DA or LA elements) and of the processes which deposited them. Additionally, the juxtaposition of channel belts originated from a common river allows to recognize in the studied succession two channel-belt-complex styles (Styles 6 and 7) depending upon the degree of incision and amalgamation of channel belts along the exposures (e.g. moderately to weakly amalgamated).

5.3.1. Alluvial architecture style 1

Multistorey, sheet-like channel belts dominated by downstream accretion. These sandbodies have sharp and ondulatory basal surfaces; lateral sandstone-body margins can be either slightly incised wedge-shaped pinchouts (< 1.5 m high, 10–25 m wide) onto fine-grained components, or vertically incised as much as 4 m into previously deposited sediments. Palaeoflow dispersion is generally low (< 30°) around the mean (Fig. 7A). Multistorey sandbodies consist of a stack of multistory sandstone ribbons and sheets, which are predominantly composed of downstream accreting elements (DA-CDA). Single channel-fill deposits display isolated ribbon or sheet geometries, are up to 5.5 m thick and 20–350 m of true width; the larger deposits represent channel belts instead of single channels. Channel belts in the cluster contain multiple, asymmetrical, internal scours at bases, overlied by a 20–50 cm thick gravel lag (facies Gm) that evolve to a sandstone-dominated package containing large-scale inclined surfaces (DA element) and tabular units of sandy materials (SB element), with abundance of laminated sandstones (SL element) toward the top (Fig. 7B). In some stories the described facies succession fine-upwards, and evolve to massive, silty sandstones with minor than 60 cm thick (facies Fm or Tm) interbedded with rippled sandstones (Sr facies).

Interpretation: The sheet-like external and internal geometries, overall low dispersion of paleocurrent direction, dominance of coarse-grained sediments, lack of evidence of lateral accretion, presence of erosional bases and channelized nature of the infilling all indicate deposition within low-sinuosity alluvial channels. On the basis of external and internal geometries, channels were up to 6 m depth, but typically between 3 and 5 m, and sediment accumulated by the lateral shifting of

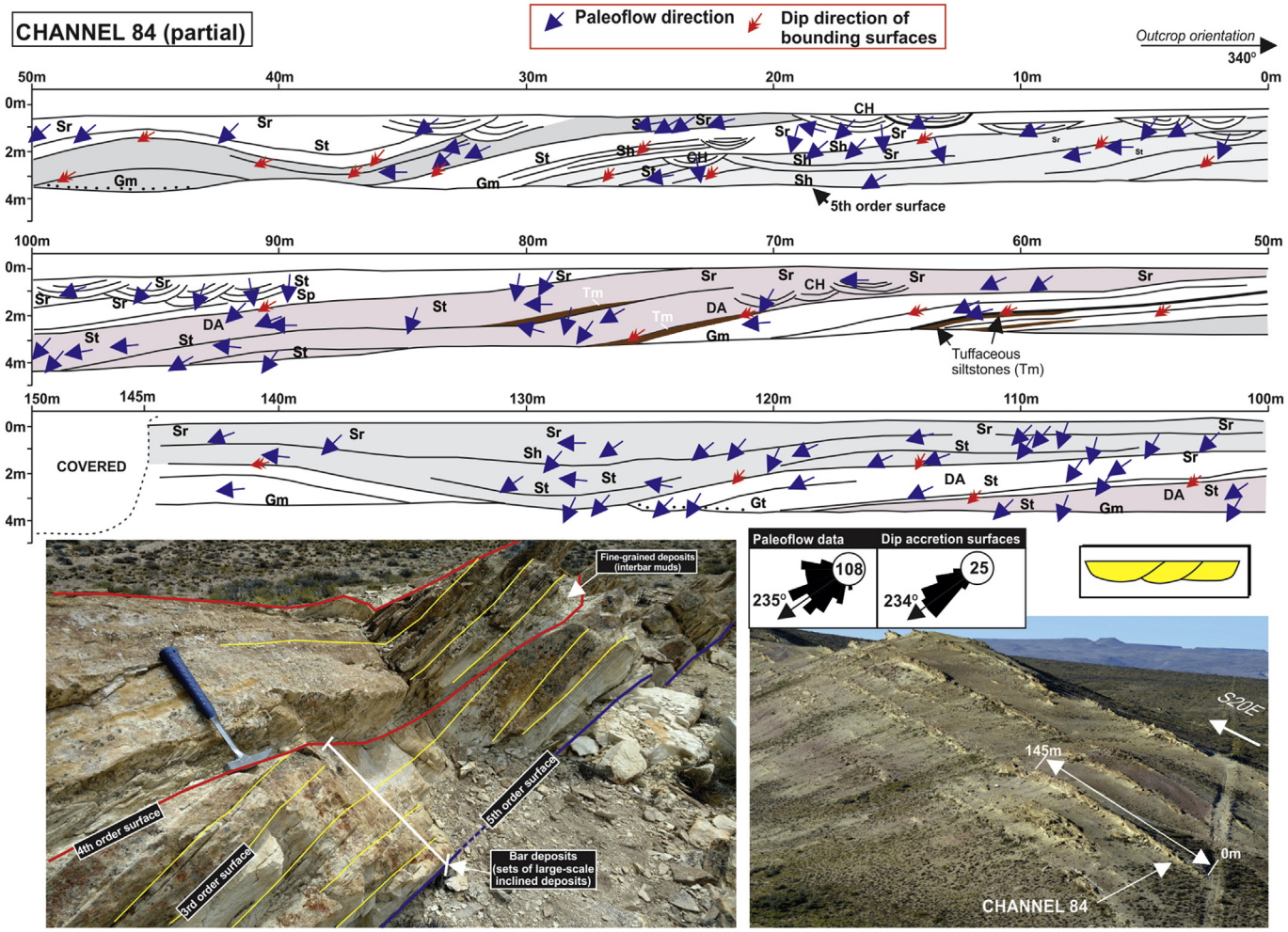

Fig. 8. Alluvial architecture style 2: Multilateral, low-sinuosity channel belt dominated by downstream accretion (DA). Section B, northernmost part of the study area. Abundance of DA elements is evidenced by the comparable direction of dips of accretion surfaces and paleoflow data obtained from cross-bedding. Code of facies is in Table 1. The inset shows a schematic summary indicating main features.

channels across a broad channel belt. Preservation of massive siltstones below of erosional surfaces in multistorey sandbodies reflects abandonment and successive relocation after avulsion (see Fig. 6B). Most of DA elements are bars attached to a channel margin, with few examples of mid-channel bars of a braided river. From this, we consider that majority of the channels are integrated by alternate bar complexes along the channel margin and associated to a low-sinuosity thalweg (Miall, 1996).

5.3.2. Alluvial architecture style 2

Multilateral, sheet-like channel belts dominated by downstream accretion (DA element). This style has been identified in two (2) channel belts of Section B, and consists of couplets of: i) subordinate, erosionally based, sandy downstream-accretion large-scale strata (DA-CDA elements), that upward grade to ii) fine-grained sandstone wedges consisting of centimeter-scale ripple laminated and horizontally laminated siltstones. Rippled sandstones and fine-grained sediments (Fig. 8) make up to 40% of the sandstone package, and their deposits are laterally continuous in the top of the channel belts. Channels were relatively narrow (30–45 m of width and 2.5–3.5 m thick) compared to the resultant channel-belt widths, with flow depths that correspond to the full height of the channel belt (~3.5 m). Some of the DA packages are truncated by an erosion surface overlied by Sla and St facies that pass up to rippled sandstones (Sr facies), reflecting small channel fills, likely chute channels.

Interpretation: The dip direction for downstream accretion macroforms and palaeoflow data of the stories indicate bar deposits in a low-sinuosity stream with predominance of sandy bedload. The upper part of the stories reflects low-energy depositional conditions that could either represent gradual abandonment of channels or a long-lasting, low-energy channel belt in a marginal position of a larger-scale channel belt. Channel fill (CH elements) indicate small and narrow channels, but the resulting channel belt can reach up to 630 m of true width and about 4.5 m of maximum thickness, evidencing lateral coalescense of stories with a multilateral arrangement (Potter, 1967; Gibling, 2006). Lack of levee deposits, as well as flat tops of the channel belts reflect very low rates of subsidence, resulting in relatively high W/T values, in the range of broad sheets. These sandy, bedload-dominated streams were deposited in regions of a very low channel slope and relatively uniform rates of sediment supply.

5.3.3. Alluvial architecture style 3

Sheet-like channel belts dominated by lateral accretion (LA element). This style is characterized either by sandstone channel belts consisting of several lateral stories with internal truncations and flat tops, or by narrow abandoned channels on the top of the channel belt, then filled with tuffaceous mudstones. All the examples of this style (n = 11, around 5% of the channel population) occur in Section B.

The typical record of bedsets, which contains a basal coarse-grained channel lag (facies Gm) overlying a shallow (< 50 cm) scour, is mainly made up of sediment deposited by plane bed (facies Sl) and migrating dunes (St and Sla facies), with interbedded rippled sandstones (facies

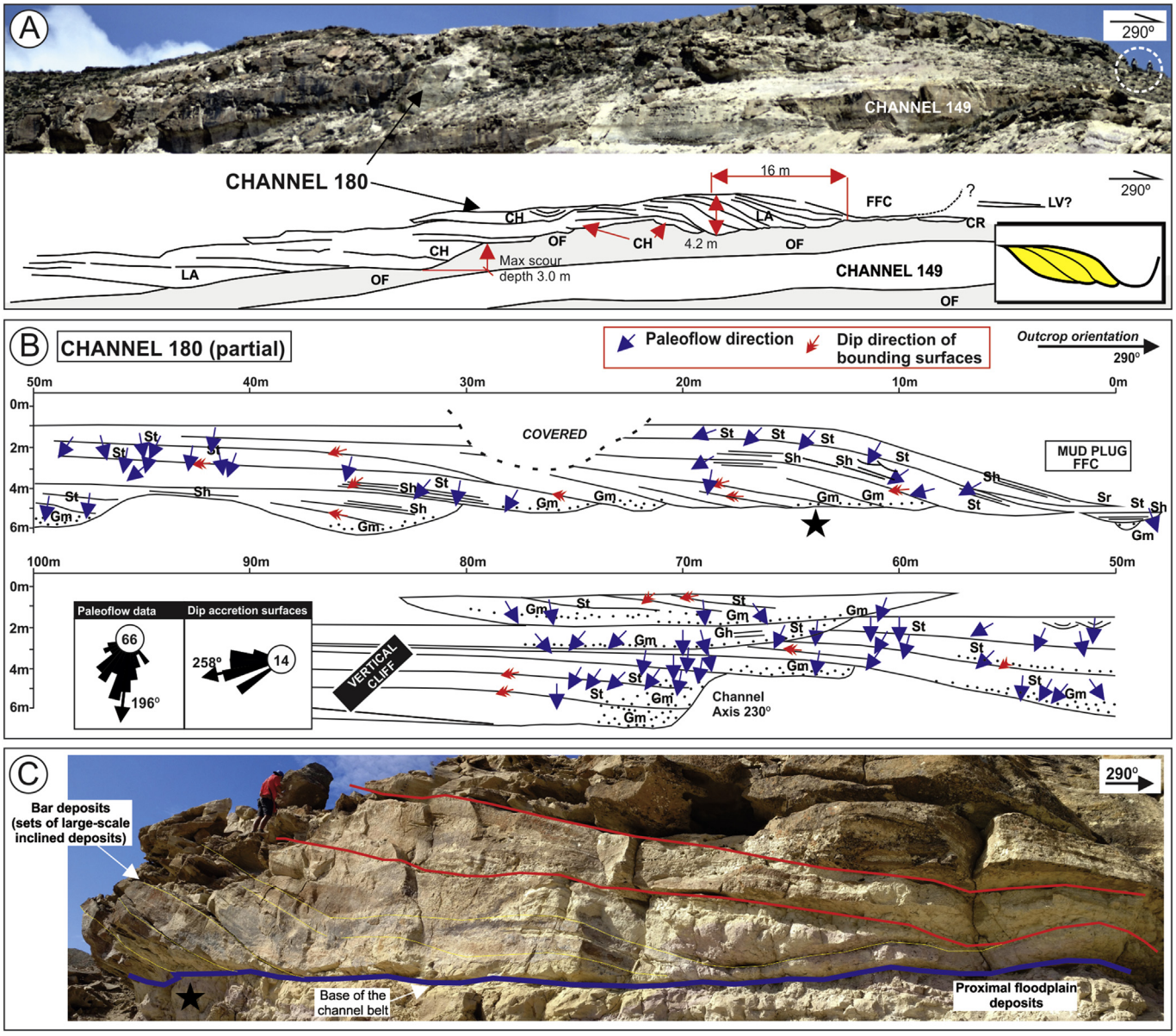

Fig. 9. Alluvial Architecture style 3: Sheet-like channel belts dominated by lateral accretion (LA Element). **(A)** Original photomosaic of outcrop (Channel 180) and photo interpretation. Note the stacking of lateral accretion deposits of upper stories in the NNW (right) channel belt margin, making up the main thickness of the channel-belt (up to 4.2 m thick). The inset shows a summary diagram with main attributes. **(B)** Line-drawing and involved facies of part of the meandering channel belt (Channel 180). Abundance of LA elements is evidenced by the high angle between the dip direction of accretion surfaces and paleoflow data on cross-bedding (inset). Code of facies is in Table 1. **(C)** Field example of lateral accretion bar deposits (bedsets). Coloured lines are surfaces, with thicker lines indicating more significant surfaces. The black start marks the position of the features in the 2D panel of Fig. 9B.

Sr) and plane-parallel fine-grained sandstones (facies Sl) on top of the lensoidal bar-accretion set (Fig. 9). Identified bedsets range in thickness between 2.5 and 4.2 m, while the apparent width of single point bars (measured from the shallow part of the channel toward the coarse-grained basal lag) ranges between 16 and 40 m. The example shown (Fig. 9) has a W/T aspect ratio of ~75 and constitute one of the widest channel belt located on the vertical cliff on top of the Cerro Ballena.

Interpretation: This channel-belt architecture reflects deposition by relatively large, stable, sinuous, mixed-load rivers that deposited sand in point bars and, locally, silt in abandoned channels. The low number of stories of the channel belt indicates that the river was relatively stable, possibly reflecting a consistent discharge regime during deposition. Although there may be some slight adjustment for compaction, the relief of fully preserved bar clinoforms can be used for the estimation of paleoflow depth of meandering rivers (Allen, 1965; Mohrig et al., 2000). Thus, the represented channel (Fig. 9) have had a local flow depth up to 4.2 m.

5.3.4. Alluvial architecture style 4

Channel belts containing ribbon-shaped fixed channels with attached splays. Type 4 channel belts are not common but occur, in Section A, representing ~1% of the analyzed channels. These sandbodies are almost symmetrical in cross section, and exhibit attached splays on both sides of the main channel fill (Fig. 10). The bases of the channels are defined by broadly symmetrical scours that cut into sheet siltstones, and extending up to the points of splay attachment on either side. In Fig. 10 no mud plug occurs at the top of the channel belt, that contains a single sandy story filling the channel with a W/T ratio of 8. Paleoflow data from cross bedded (St) indicate a drainage towards the thalweg, with paleocurrents oriented into the outcrop. Toward the top

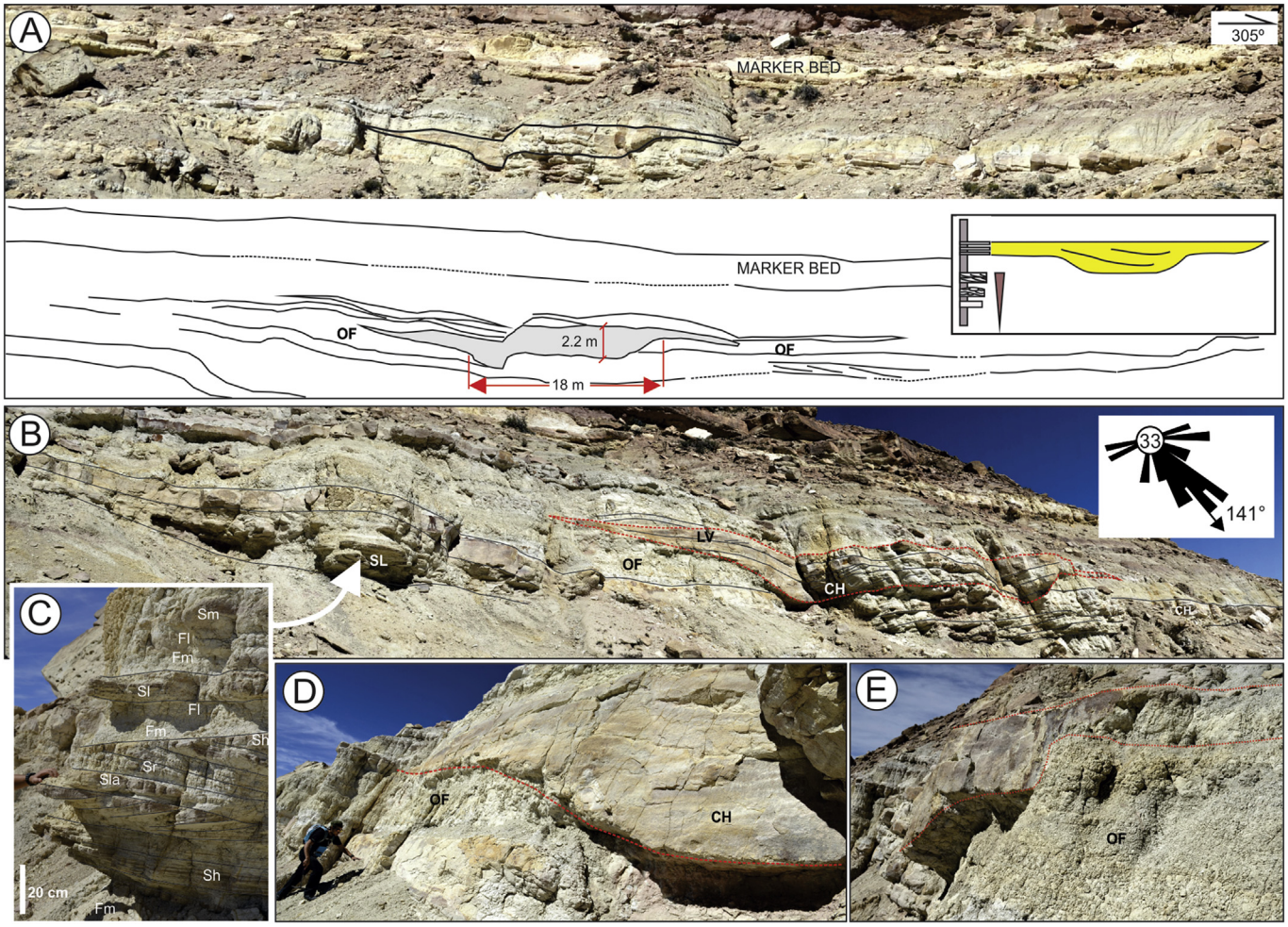

Fig. 10. Alluvial architecture style 4: Channel belts containing ribbon-shaped single channels with attached splays. **(A)** Original photomosaic, photointerpretation overlying the photomosaic, and simplified sketch (inset). **(B)** Detailed bedding and architectural elements. Code of facies is in Table 1. **(C)** Facies arrangement of proximal floodplain deposits (SL and CR elements) underlying the selected channel belt. **(D–E)** Views of the basal scour of the ribbon channel.

of the channel belt the facies pass into low-angle cross-bedded sandstones (Sla) and massive sandstones (Sm). Laterally, architectural elements CR and CS are fully preserved. When identified, bar migration is roughly parallel to the paleoflow (DA element).

Interpretation: Single-story, narrow and broad ribbon sandstone bodies are interpreted as deposits of low-sinuosity, fixed channels that produced DA elements during higher-magnitude discharge events, intimately associated with the floodplain deposits within which they are encased. Overbank flooding during higher-magnitude discharge events produced splays attached to the CH elements forming a levee (LV element). Preservation of levee deposits reflects a high rate of subsidence during and/or shortly after the deposition of this type of channel belt, which provided short time for aeolian and rainfall erosion processes to planate the levees (Wilson et al., 2014).

5.3.5. Aluvial architecture style 5

Ribbon or sheet-like channel belts dominated by resedimented volcaniclastics. This style of deposition is found in five channel belts, including the distinctive pale-grey to white marker bed (MB in Fig. 3) located near the base of Section B (Fig. 11A). In the marker bed, the volcaniclastic succession starts with a 0.7–1 m thick tuffaceous siltstone (Tm and Tl facies) identified along the western limb of the anticline. Overlying this level, the strata show planar bases and consist of a 0.3 m thick package of coarse to medium-grained plane-laminated sandstones (Sl) containing isolated pebble clasts and grain-size inverse grading, followed upward by a 3–4 m thick, matrix supported, largely disorganized tuffaceous conglomerate (Gmv facies) disposed in tabular bodies. Root traces are recognized on top of the tuffaceous siltstones, eroded by the coarse-grained package. Whereas the bases are planar, the top of the marker bed is irregular due to subsequent erosion. Conglomerates are predominantly composed of pebble-sized, sub-angular components with a maximum clast size of 10 cm (mean around 2 cm) suspended in an ash-dominated, poorly sorted (cineritic to sandy) matrix, with variable content of sub-angular lithic fragments (< 2 cm in size) (Fig. 5J). Towards the top of the marker bed, sandy volcaniclastic strata containing horizontal bedding (Sl) and fining-upward trend are preserved. Although elongated conglomerate clasts have their *a*-axis parallel to the basal boundary, no imbricate clasts were observed.

The remaining examples of channel belts of this style are thick channels (between 5.2 and 6.4 m of thickness) characterized by massive sandstones (Sm facies), minor Sl facies and rare diffuse St facies, with Gm facies overlying an erosive base (Fig. 11B and C).

Interpretation: This style of architecture is associated to channels that were occupied by debris flows and hyperconcentrated flood flows, likely associated to intense rain events during periods of distal volcanic activity. Tabular deposition of fine-grained tuff (Fm and Tl facies) in low-slope subaerial environments reduces the infiltration capability of substrates, favouring overland runoff and flashiness of the discharge of coeval rivers. The massive, matrix supported conglomerate (Gmv) and associated facies are either interpreted as debris flows or volcanic mudflows infilling shallow channels, both processes associated to the reworking of volcanic particles by cold water.

Fig. 11. Alluvial Architecture style 5. Channel belts dominated by resedimented volcaniclastics. **(A)** Tuffaceous marker bed (MB in Fig. 3) at base of Section B (*sensu* Figari et al., 1998). A fine-grained vitreous tuff at base (Facies Tvl, star) is covered by a 4,2 m thick, poorly-organized tuffaceous conglomerate (Facies Gmv). People is 175 cm tall. **(B)** Ungraded, massive infilling of the channel fill. Jacob staff is 1.5 m long. **(C)** Channel margin, overlying a volcaniclastic floodplain. Diffuse plane-parallel is evident, although there is no vertical gradation in grain sizes. Hammer is 30 cm long.

Poor sorting, lack of low flow-regime sedimentary structures, presence of matrix-supported fabric and comparatively thick beds are characteristics of subaerial mudflows/debris flows documented from both ancient and modern environments (Nemec and Steel, 1984; Smith and Lowe, 1991; Thouret and Lavigne, 2000). Diffuse horizontal laminations at base and toward the top could be due to hyperconcentrated flood flows (Smith, 1986; Sohn et al., 1999) in rapidly aggrading conditions. Debris flows are associated to distal volcanic activity, with source areas located to the west (Umazano et al., 2009), being preceded by pyroclastic air-fall deposits in the study area. A major sedimentological consequence of this volcanic activity in the Andean volcanic arc is the observed change in the floodplain composition of Section B, which record a change in the nature of the sediments transported as wash load by the rivers. The paucity of primary pyroclastic fall deposits and dominance of resedimented particles in fine-grained floodplain facies of Section B evidence successive reworking and removilization of ash-particles in upstream catchment areas (Kataoka, 2009). The former interpretation of ignimbrite deposition associated to the marker bed (Bridge et al., 2000) is rejected due to the lack of evidence of transportation in hot conditions (fossil fumarole pipes, carbonaceous wood fragments, pink coloration, welding, flattened pumice clasts or eutaxitic textures in thin sections), being their particular features integrated into the fluvial system as the record of a channel belt filled by volcaniclastic particles during high-magnitude floods.

The remaining thick, ribbon channel belts of Section B (see Fig. 12 for distribution) represent trunk channel systems that delivered large quantities of loose volcaniclastic sediments to the floodplain during floods.

5.3.6. Alluvial architecture style 6

Unconfined, isolated to poorly amalgamated sheet complex. This architectural style consists of multistorey, downstream accretion (DA element) dominated channel belts of styles 1, 3, 4 and 5 with broad ribbon or narrow sheet geometry, surrounded by fine-grained (siliciclastic mudstone and siltstone) deposits. It's typical of Section A, but also occur in some intervals of Section B (see Fig. 12). Limited physical connectivity with other channel belts reflects the development of channel belts on wide floodplains (Fig. 5L).

Interpretation: The large vertical spacing and small width of channel belts is interpreted to be either the product of higher subsidence rate or increased floodplain aggradation rate in relation to in-channel aggradation (Legarreta et al., 1993; Martinsen et al., 1999; Catuneanu, 2006), which gave few opportunities for rivers to migrate and expand for a greater period of time before avulsion.

5.3.7. Alluvial architecture style 7

Unconfined, moderately amalgamated sheet complex. This style of alluvial architecture occurs in Section B and it is characterized by the development of interconnected multistorey sandstone broad ribbons and narrow sheets. They are predominantly composed of downstream-accreting barforms, with scarce lateral accretion (Styles 1, 2, 3 and 5) intercalated with thinner overbank facies. Channel belts in the cluster (Fig. 12) contain multiple internal scours, and the uppermost channel belt could contain a concave-upward surface filled with a mud plug (as shown in Fig. 9A). There is a large lateral variation in geometries (width, thickness) of the channels in the cluster, but the complex is dominated by downstream accretion. Although scarce, some

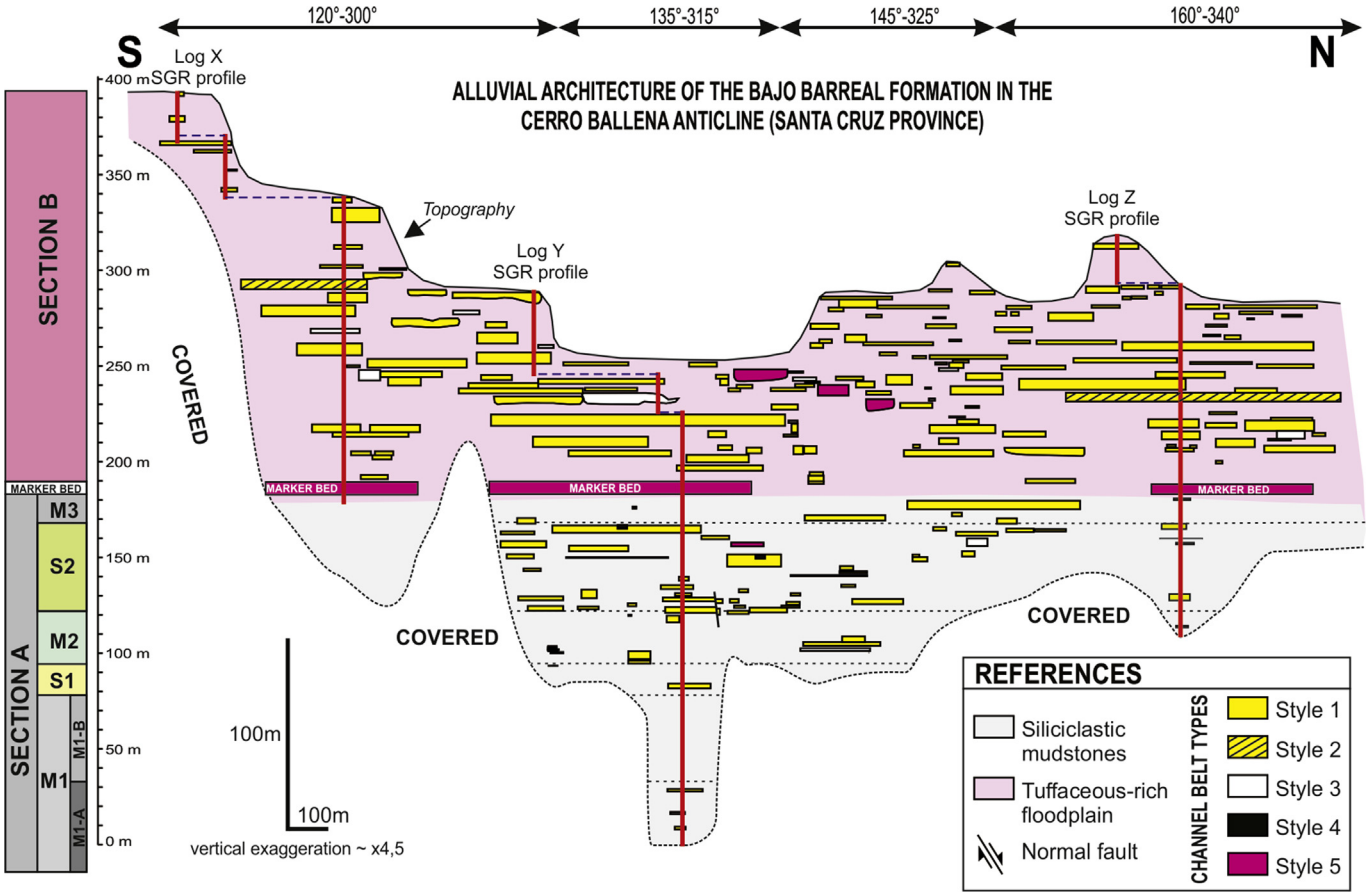

Fig. 12. Panel showing the mapped stratigraphy and facies architecture of the Bajo Barreal Formation along the western flank of the Cerro Ballena anticline. The represented widths of channel belts are the apparent data. Major subdivisions of Section A are indicated. Channel belts from Section A are mainly isolated (Alluvial architecture style 6) and of small scale, whereas channel belts of Section B are of larger scale and have moderately high connectivity (Alluvial architecture style 7).

sandbodies in the complex have overbank mudstone deposits near to the channel-belt margin.

Interpretation: Stratigraphic intervals of multistory and multilateral, amalgamated sheet-like channel belts with minor overbank deposits are interpreted to record low rates of accommodation space creation (Miall, 1996; Catuneanu, 2006). Lateral occurrence of channels with different sizes and planform shapes suggests the occurrence of coeval rivers that carried very different discharges, features distinctive of anastomosed (Makaske, 2001) river systems or anabranching fluvial systems (Nanson and Knighton, 1996; North et al., 2007). Predominance of downstream-accretion bedsets and lack of large-scale erosional surfaces reflect that the low-sinuosity river systems were not confined within a valley.

6. Alluvial organization

In this section, we summarize the directional data of paleoflow measurements, and the geometrical information obtained of channelized deposits, which constitute a useful information for oilfield development. Furthermore, paleohydrological estimations are presented.

6.1. Palaeocurrent analysis

A total of 3777 paleocurrent measurements were obtained from 218 channelized deposits, which allows to define 218 mean paleoflow vectors (Fig. 13A). The average paleoflow direction using the entire set of data is unimodal toward 187° (StD = 45°), while the distribution of mean paleoflow vectors of channels shows a bimodal distribution, with a main vector pointing SSW (185–200°), and a secondary mode toward SE (~140–150°). The classified rose of mean paleoflow vectors (Fig. 13B) shows that the main contribution to the mode is associated with sandbodies included in Section B. The rose diagram with radius proportional to maximum thickness (Fig. 13C) amplifies the secondary mode toward SE (~150°), which is associated to channels up to 4 m thick. Moreover, thickness-weighted rose shows low palaeoflow dispersion of the channel belts, rarely with palaeoflow vectors toward NE. Some of those unusual channels that flowed toward NE presumably were the source of published palaeoflow data (Bridge et al., 2000, their Fig. 6), but still there is a large difference between the mean paleoflow vectors of this study (187°) and those indicated by Bridge et al. (2000), where a mean vector of 82° was reported.

The paleoflow distribution toward the SSW (Az = 187°, n = 3777) is consistent with the occurrence of a southward depocenter. Two main NW-SE neocomian half-graben depocenters located southward of Río Deseado were previously interpreted using surface mapping (Figari et al., 1998: Fig. 4); although their tectonic evolution and sedimentary infill remain unknown up to date. Palaeoflow vectors toward NNE, NNW and NE identified adjacent to channels flowing SSW reflect both channel sinuosity (as indicated by curved meanders) or avulsion directions in a flat geomorphic scenario (see below).

6.2. Geometrical analysis of channelized deposits

218 sandbodies were measured during the fieldwork. The Sections A and B contain 58 and 160 sandbodies, respectively. In order to identify temporal (vertical) changes in the behavior or geometries of the fluvial system, the Section A was divided into five stratigraphic sub-units (Fig. 3) according to its “mud-sand” ratio (M1, S1, M2, S2 and M3, in ascending order).

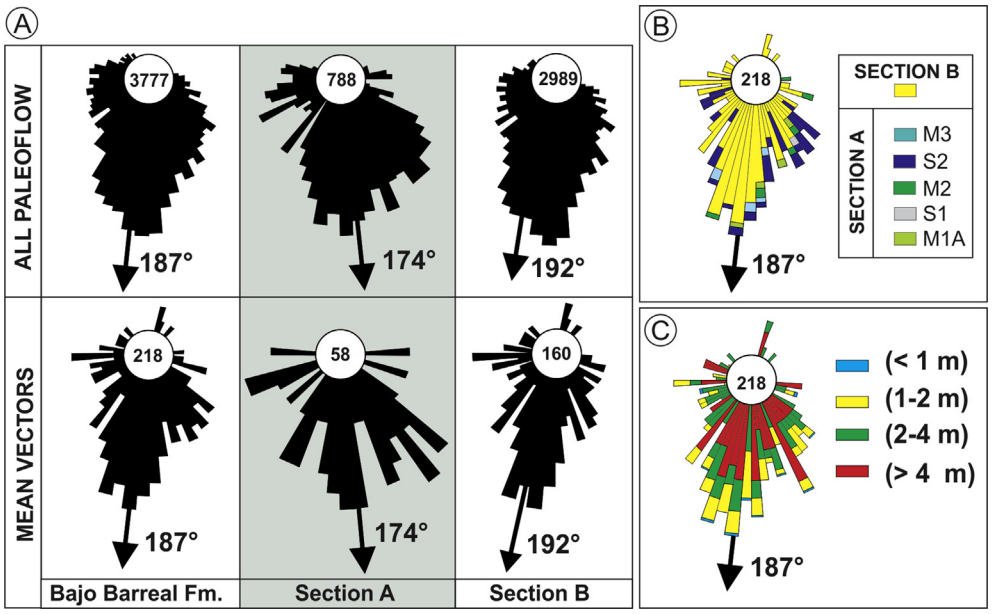

Fig. 13. (A) Rose diagrams summarizing palaeocurrent data of the Bajo Barreal Formation in the Cerro Ballena anticline, with distinction of data obtained in channel belts within the Sections A and B. Data using the mean vector of the channels reflect transportation toward SW-SE, subordinate transport toward W-WNW and rare data toward NE. **(B)** Rose diagram of mean paleoflow vectors classified according to their stratigraphic positions (subdivisions of Section A shown in Fig. 3). **(C)** Rose diagram of mean paleoflow vectors weighted according to their maximum thicknesses.

6.2.1. True width (W)

For the entire dataset, true width (W) of channel deposits ranges from 2.8 m to 629.7 m, with a mean W of 57.5 m, while apparent width of sandbodies ranges from 8 m to 771 m with a mean W of 97.9 m. Mean apparent width obtained by Bridge et al. (2000) is razonably close (112.87 m). The mean true width of sandbodies within Section A is 45.7 m, reaching a maximum value of 177 m (Fig. 14A), whereas channels from Section B show a mean true width of 61.1 m and a maximum value of 629.7 m. The vertical distribution of geometries within Section A shows an increase of true width (W) throughout the unit (Fig. 14E). Channels within the M1 sub-unit have an averaged mean W of 18.8 m, while channels within M3 sub-unit show an averaged true width (W) of 68.7 m. The mean width of channels of M3 sub-unit are quite similar to the mean width of section B (W mean = 61.6 m).

6.2.2. Maximum thickness (T)

Maximum thickness of all sandbodies ranges from 0.4 m to 8.7 m, with a mean T of 2.5 m. Channels within the Section A show a general upward increase in T from sub-unit M1 (T mean = 1.3 m) to sub-unit M3 (T mean = 2.7 m) (Fig. 14E). The mean thickness of M3 is quite similar to those of channelized sandbodies within Section B (2.6 m). The comparison of frequency histograms of channels between Sections A and B reveals a high percentage of observations in the same interval of thickness (white circles in Fig. 14B), likely evidencing a hierarchical organization of large trunk channels and minor-scale tributaries in the fluvial system. Furthermore, Section B contains a second mode in the histogram around 5.5 m of thickness (12 sandbodies), representing the scale of the main trunk channels of the involved fluvial system.

6.2.3. Width/thickness ratio (W/T)

Sandbodies are mainly narrow sheets or broad ribbons that have an averaged W/T ratio of 24.4, with minor differences between Section A (W/T = 21.1) and Section B (W/T = 25.5) (Fig. 14C). As mentioned, both W and T of sandbodies of Section A gradually increase from sub-unit M1 to sub-unit M3, a trend only modified in sub-unit S1, which contains a single, large-scale sandbody that depart from the vertical trend of sizes (Fig. 14E). With this single exception, channels of Section A display a widening and thickening upward trend. The W/T crossplot (Fig. 14D) reflects channels with variable shape and scale flowing in the study area during deposition of each sub-unit of Section A, and within Section B, implying variable discharge of the involved rivers. A likely fluvial system with main (trunk) rivers and tributaries of different scale is envisaged from the distribution of scales and geometries.

6.3. Palaeohydrological estimations

Set thicknesses of cross beds were measured within eleven fluvial channels of Section A, and in thirty channels of Section B, and estimations of several key parameters were obtained (Table 2). For each channel, we measured between 4 and 11 cross sets. Although the calculated values should not be considered as absolute values, they allowed to compare the vertical (temporal) evolution of the fluvial system.

Based in the estimations, channels record an increase in both average flow depth (d_m) and mean channel width (Wc) from Section A (d_m = 4.05 m; Wc = 45.5 m) to Section B (d_m = 5.76 m; Wc = 69.5 m). The mean true width, calculated using GPS and palaeoflow data, indicate that channels of Section A have 45.7 m (n = 58), while channels of Section B show a mean value of 61.1 m (n = 160) (Fig. 13B), showing a very close correspondence with mean channel width values obtained using palaeohydraulics (Table 2). This convergence of results from two independent sources of information collaborates in strengthening the geometric analysis of sandbodies.

Although calculations of average daily discharge (Qm) using two independent methods show large disparity in the absolute values (Table 2), both approaches show that the resulting Qm values for channel belts of Section B are higher than those obtained for Section A. As discharge values reflect the size of the catchment area (Van der Neut and Eriksson, 1999), it is inferred that larger rivers on an increasingly broad fluvial system developed upward; stream power would also have increased with an enhanced volume of water derived from the larger catchment area (A_d).

Moreover, palaeoslope (S) estimations were very close to the maximum gradient of 0.0070 m m^{-1} for rivers proposed by Blair and McPherson (1994), but far of the 0.026 m m^{-1} value for modern alluvial fans. Furthermore, the resulting parameters for drainage area (A_d) show a ~3 times increase in the catchment area of rivers of Section B in relation to those of Section A. Such increase could be associated to stream capture or enlargement of the drainage basin, and could be a potential reason of the change in the composition of the fine-grained sediments delivered via wash load to the distal floodplain.

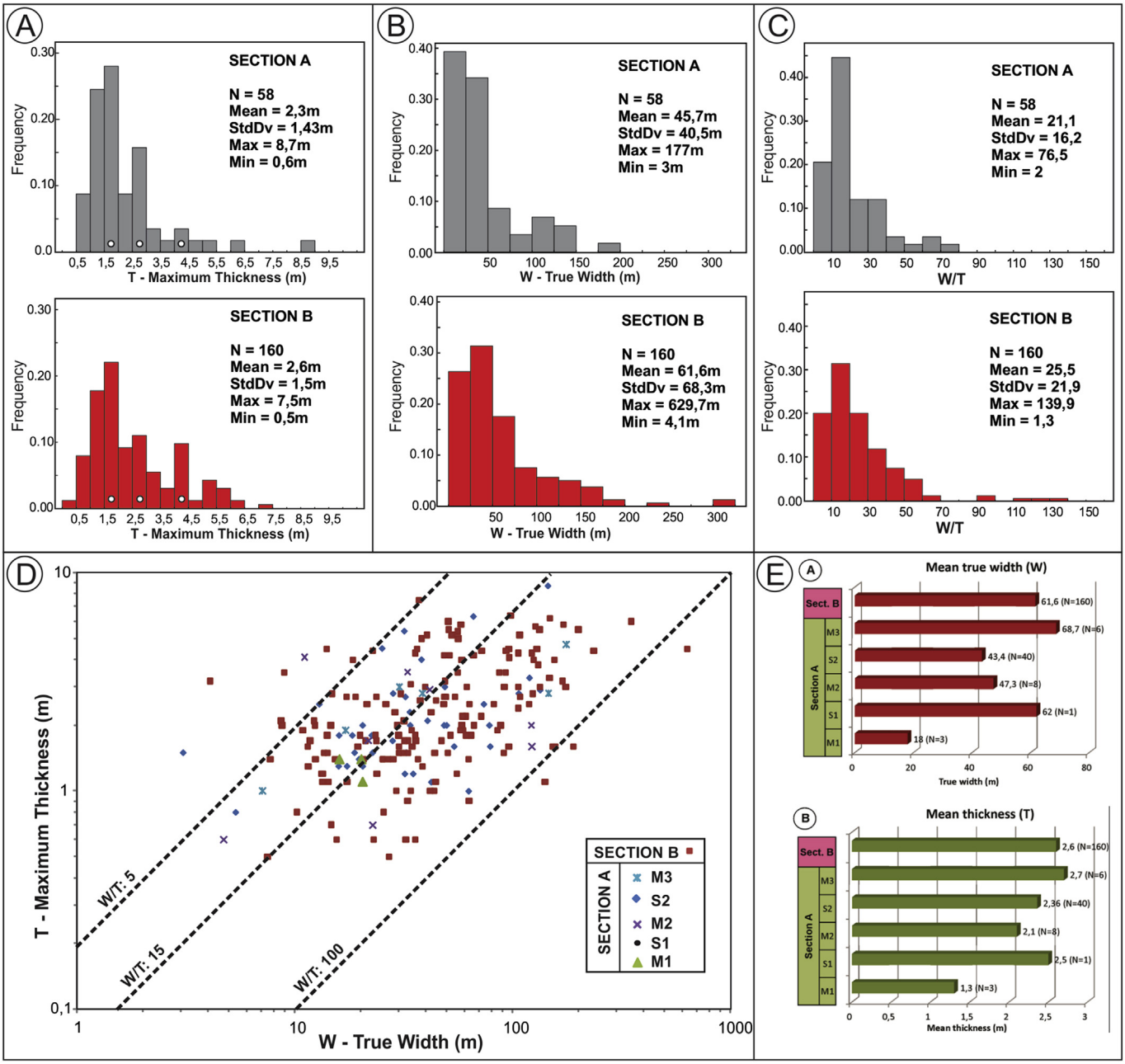

Fig. 14. Comparative histograms of **(A)** maximum thickness, **(B)** true width, and **(C)** W/T ratio from channelized sandbodies of Sections A and B of the Bajo Barreal Formation in the Cerro Ballena anticline. A multilateral channel belt of 629 m of true width is not represented in (B). **(D)** W/T ratio of fluvial sandbodies of the Bajo Barreal Formation in Cerro Ballena anticline. **(E)** Vertical (temporal) variations in W and T of fluvial sandbodies of the Bajo Barreal Formation at Ballena Hill. Note the vertical increase of T along Section A and the comparable external geometry of channels between the M3 sub-unit of Section A and Section B.

7. Discussion

7.1. Depositional model

The alluvial deposits of Section A (*sensu* Figari et al., 1998) are associated to perennial rivers and are multistorey, with ribbon or narrow sheet geometries, and dominated by downstream accretion of low-sinuosity channels, with rare fixed channels. Proximal floodplain deposits are commonly preserved below and in the margins of channel belts. The lack of levels containing well developed paleosols suggests that movility of the channels was relatively high or that aggradation of the floodplain was high. The channel belts are physically isolated evidencing very-low interconnectivity, and separated from superjacent channel belts by several meters to tens of meters of overbank fines, suggesting high rates in accommodation creation in relation to sediment supply (high A/S ratio, cf. Martinsen et al., 1999). The wide variety of channel sizes in Section A suggests the presence of rivers that carried very different discharges, where the largest channels are inferred as deposits of major trunk rivers, whereas smaller channels of variable size and planview geometry are inferred as tributaries or floodplain drainage channels in a multichannel system (Fig. 15). Current classifications for multichannel fluvial systems that show variations of styles and geometries of the involved channels across the channel belts are commonly referred to some type of anabranching style (Nanson and Knighton, 1996) but can also be referred to contrastyle, plural sedimentation systems (*sensu* Lewin and Ashworth, 2014). Low-sinuosity channel of Style 4 contain the attributes of typical anastomosed rivers (Makaske, 2001; Stouthamer and Berendsen, 2001,

Table 2
Summary (average) of paleohydrological data derived from cross-bedded set thickness measured in 41 channels of Sections A and B of the Bajo Barreal Formation. Notice the increasing of channel width in Section B, also detected using GPS measurements, with comparable values. Flow depth, daily discharge and bankfull channel depth also increase in Section B.

	Section A (n = 11)	Section B (n = 30)
Cross-set thickness (range, average)	7–30 cm; 18 cm	8–66 cm; 24.5 cm
Mean dune height (h_m) [a] (range, average)	18–88 cm; 52 cm	25–194 cm; 74 cm
Mean Flow Depth (d_m) [b] (range, average)	155–707 cm; 405 cm	432–720 cm; 576 cm
Channel Width (w_c) [c]	45.5 m	69.5 m
Average daily discharge (Qm) [d]	133 m^3/seg	421.59 m^3/seg
Mean bankfull channel depth (d_b) [e]	4.90 m	6.52 m
Bankfull channel width (w_b) [f]	84.5 m	126.91 m
Average daily discharge (Qm) (2nd method) [g]	53.77 m^3/seg	111.13 m^3/seg
Palaeoslope (S) [h]	0.007847 m/m	0.006344 m/m
Mean bankfull water discharge (Qb) [i]	1748 m^3/seg	4072 m^3/seg
Drainage area (A_d) [j]	23,700 km^2	78,923 km^2
Principal stream length (L) [k]	525 km	1006 km

[a] $h_m = 5{,}3\beta + 0{,}001\beta^2$, $\beta \equiv Sm/1{,}8$, Sm = mean cross-set, h_m = mean dune height (Leclair and Bridge, 2001; Leclair, 2002).
[b] $6 < d/hm < 10$ (d = mean flow depth) (Bridge and Tye, 2000).
[c] $Wc = 8{,}88\, dm^{1{,}82}$, dm = 0.5 d (Bridge and Mackey, 1993).
[d] Qm = v.A (v = velocity necessary for dune migration, a velocity of 0.75 m/seg is assumed).
[e] $d_b = 0.6\, M^{0.34} Qm^{0.29}$ (Schumm, 1969).
[f] $W_b = 8.9 d_b^{1.40}$ (Leeder, 1973).
[g] $Qm = 0.027 w_b^{1.69}$ (Osterkamp and Hedman, 1982).
[h] $S = 60\, M^{-0{,}38} Qm^{-0{,}32}$ (Schumm, 1968) supposing M = 10 (corresponding to mixed-load palaeochannels with sinuosity $S < 2$).
[i] $Qb = 4.0 A_b^{1.21} S^{0.28}$ where $Ab = d_b x W_b$ (Williams, 1978).
[j] $Qb = Ad^{0.75}$ (Leopold et al., 1964).
[k] $L = 1.4 Ad^{0.6}$ (Leopold et al., 1964).

2007; Makaske et al., 2007). The main mechanism of migration of channels of Section A is considered autogenic avulsion produced by either progradation of channel belts onto proximal floodplain deposits or by rapid relocation of the channel belt over distal floodplain deposits (see below). The dispersal pattern shows a consistent SSW-SSE palaeoflow direction (Fig. 13A) and reflects the location of a depocenter southward of the study area.

The alluvial deposits of Section B are characterized by sheet-like channel fills with higher interconnectivity, encased in thinner, tuffaceous floodplain deposits. Channel belts are mainly multistory packages dominated by downstream accretion, although meandering rivers are frequent. As in Section A, there is a large variation in thickness, width and external geometry of the sandbodies, reflecting variable discharge of the involved rivers. Moreover, paleohydraulical estimations indicate an increase in the discharge, flow depth and width of rivers of Section B (see Table 2), which also exhibits a larger proportion of conglomerate facies evidencing flows of higher energy. Amalgamated channel-belt clusters of large channels along particular stratigraphic intervals of Section B are interpreted as periods of lower accumulation rate relative to avulsion rate of the trunk river (Bridge and Leeder, 1979; Shanley and McCabe, 1994), and can be considered a low-accommodation system tract characterized by elevated connectivity of channel belts (Martinsen et al., 1999). Most of the analyzed fluvial channels relocated in the floodplain by avulsional processes (see below). Paleoflow data during deposition of channel of Section B evidence the continuity of the paleotransport toward SSW (Fig. 13). The suite of attributes identified (avulsion-dominated rivers, common overbank sedimentation, channel banks resistant to erosion by cohesion, and aggradational setting) are typical attributes of anabranching rivers with high variation in rainfall distribution and humid climates (Nanson and Knighton, 1996; North et al., 2007). Different river styles (low-sinuosity, meandering, anastomosed) of different scale were identified in the Section B, compatible with contra-style, plural sedimentary fluvial systems (Lewin and Ashworth, 2014).

7.2. Migration mechanisms

Detailed channel belt internal architecture (Styles 1–5) and two different styles of stacking of channel belt complexes (Styles 6–7) provide information of channel belt migration processes and mechanisms of re-occupation. We have found a low proportion of channel belts containing lateral accretion surfaces of meandering rivers (Architecture style 3, about 5% of the analyzed channel belts) or fixed channels in the floodplain (Architectural style 4, ~1%). The multilateral behavior of the channel belts (Architectural styles 2, < 1%) is also rarely established, and resedimentation of pyroclastic particles in sheet-like channel belts is uncommon (Architectural style 5, < 3%). From this, most of the channel belts reflect downstream accretion of multistorey, low sinuosity channels, evidencing repeated re-occupation of channel depressions, likely associated to avulsion mechanisms in a multichannel fluvial system.

Three styles of avulsion have been previously documented: avulsion by channel reoccupation (avulsion by annexation *sensu* Slingerland and Smith, 2004), avulsion by incision, and avulsion by progradation

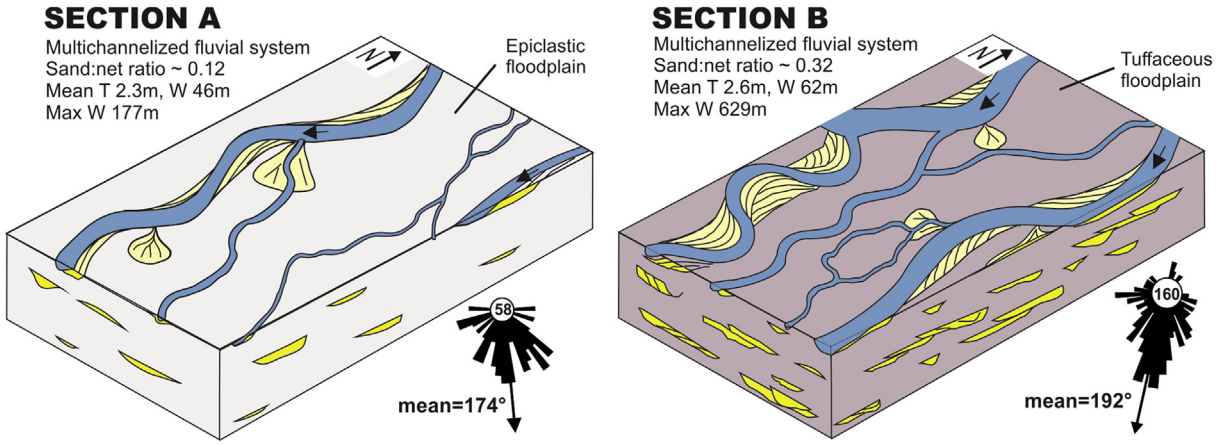

Fig. 15. Conceptual model summarizing the alluvial architecture for the Sections A and B of the Bajo Barreal Formation at Cerro Ballena anticline. For paleoflow rose the north is up to the page.

(Mohrig et al., 2000; Slingerland and Smith, 2004). From our field review, we interpreted the three styles of avulsion.

a) Avulsion by annexation: The channelized fluvial sandbodies (element CH) exhibit vertically amalgamated stories (Fig. 6B) that imply repeated reoccupation of the same site by avulsing channels (Aslan and Blum, 1999; Mohrig et al., 2000). Lenses of fine-grained floodplain deposits situated toward the top and within multistorey channel belts provide evidence for channel abandonment in relative topographic lows on the floodplain, prior to reoccupation following a later avulsion. Multistory sandbodies may cut down into CS/LV (< 1.5 m thick) or OF element. These architectures are interpreted as the record of avulsion by annexation, whereby flow-path selection takes place via channel relocalization.

b) Avulsion by progradation: Some channelized sandbodies consist of either single-story, isolated or multistory packages overlain a subjacent succession of thickening-upward or thinning-upward (e.g. Fig. 6F and H) crevasse splay beds (elements CR, CS/LV). The thickness of strata cropping out beneath the channel belt ranges between 2.5 and 8 m. The splay deposits contain weakly developed paleosols and mottled fine-grained sediments interbedded with fine to medium-grained sandstones. This alluvial organization is interpreted as the record of progressive increases in the sedimentation rate and gradual progradation of a fluvial channel into a topographically low part of a floodplain preceding avulsion ("stratigraphically transitional avulsion" of Jones and Hajek, 2007). Where an isolated channelized fluvial sandbody cuts into a subjacent succession of thinning upward-crevasse splay strata (examples in Fig. 4), this may represent a decrease in proximity to a fluvial channel prior to avulsion. However, the underlying crevasse-splay complex may still be genetically related to the overlying channelized fluvial sandbodie, since crevasse-splay complexes exhibit much lateral variation in geometries at bed scale (Smith et al., 1989; Jorgensen and Fielding, 1996; Fisher et al., 2007), directly linked to the micro-topography of the floodplain.

c) Incisional avulsion: Many channelized fluvial sandbodies consist of stories that cut directly into subjacent fine-grained, distal floodplain deposits (Element OF), without preservation of CR, CS or LV element (several examples in Fig. 4). This architecture records the abrupt introduction of a fluvial channel by avulsion and is denominated avulsion by incision (Slingerland and Smith, 2004). It indicates a period of nondeposition prior to avulsion, and sudden avulsion to areas of the floodplain that experienced slow gradual sediment accumulation (Jones and Hajek, 2007). Incisional avulsion is considered as the dominant avulsion mechanism in the analyzed exposures of the Bajo Barreal Formation, also identified as the main mechanism in other exposures of the unit (Paredes et al., 2016), as well as in the overlying Lago Colué Huapi formation (Casal et al., 2015).

7.3. Role of volcanic ash in the flow

Channel belts of Section A are surrounded by siliciclastic mudstones and siltstones; whereas in the Section B the channels are encased into tuffaceous siltstones. Floodplain construction in volcaniclastic packages of the Bajo Barreal Formation is mainly associated to reworking by water of ash-size volcaniclastic particles transported by rivers and distributed over wide floodplains during floods (Umazano et al., 2008; Paredes et al., 2016). In the Cerro Ballena, the increase in the tuffaceous participation of Section B together with an increase in proportion of channelized deposits along sedimentological logs allow to consider the role that a large influx of volcanic ash delivered by rivers might produce on the alluvial architecture. Volcaniclastic particles were delivered by both airfall and fluvial reworking of pyroclastic sediments. Both processes would lead to an increase in floodplain aggradation rate while having limited impact on channel belt aggradation rate, where bedload deposition will occur.

Heller et al. (2015) consider that major amount of ash supply would increase cohesiveness of floodplain deposits exposed in river banks, which can promote a change in river planform from braided to meandering (Schumm, 1985). Ash supply also increases the deposition rate, coupled with a change in soil geochemistry linked to changes in the mineralogy of floodplain sediments modifying the type and abundance of vegetation. Vegetation, in turn, increases bank strength, promoting the formation of single, deep channels and also can more effectively baffle-channel flow during times of flooding, increasing the sedimentation rate in the proximal floodplain (Heller et al., 2015). According to Heller and Paola (1996), an increase in floodplain aggradation rate could significantly reduce avulsion frequency, translating into a decrease in channel belt stacking density (low net sand). In summary, if the addition of volcanic ash to the floodplain was important in relation to channel belt aggradation, a decreasing in stacking density of Section B should be expected, because avulsion should be less frequent and thicker floodplain deposits could be preserved separating superjacent channel belts. Contrarily, the stacking density (or channel proportion along sedimentological logs) of Section B is higher than in Section A, evidencing that ash deposition have not played a dominant role in the alluvial architecture, or at least channel belt aggradation grew faster than floodplain aggradation, being associated to an independent control. Experimental studies (Hickson et al., 2005) and field studies (Makaske et al., 2017) on the anastomosed Columbia river established that high bedload supply causes bed aggradation, loss of channel flow capacity and increased overbank flooding and floodplain sedimentation, as well as crevassing and more frequent avulsions, being the probable reason of higher interconnectivity of channel belts of Section B.

7.4. Upstream climatic control

Most sedimentological studies in the Bajo Barreal Formation indicate perennial fluvial systems with large discharge variation in a seasonal climate (Umazano et al., 2008; Paredes et al., 2016) or ephemeral rivers (Hechem, 1997). In fluvial systems, subtle changes from humid warm-temperate to semiarid climate, and vice versa, would have altered the vegetation cover of the hinterland and thus controlled the discharge and sediment fluxes along the drainage network. In addition, an increase in the seasonality would also changed the fluvial processes acting on the depositional system. The lack of desiccation cracks, calcretes, evaporites and aeolian sediments, as well as high preservation of low-flow stage deposits in the bases of major fluvial channels indicate a perennial river system (Allen et al., 2013). It agrees with a humid or sub-humid climate during deposition, a climate inferred previously by palynological data (Archangelsky et al., 1994). Moreover, most of the channel fills contain evidences of transportation in conditions of high and low flow velocities or even transportation in upper flow-regime conditions, evidencing changes in discharge during the infill of single channels.

The detailed dataset of the external geometry of fluvial sandbodies (Fig. 14) and the paleohydrological parameters reflect a temporal increasing in the size of the channels, larger discharges and water availability (Table 2). The observation of more sinuous channels with better developed bank accretion packages in Section B, where channels and channel belts are thicker and wider, could indicate the occurrence to a major stream power locally associated to steeper topographic gradients and high channel movility (Ouchi, 1985; Schumm, 1993; Makaske, 2001). From this, we interpret a vertical (temporal) shift toward more humid and wetter climatic conditions as the main responsible of increasing in the stacking density, alvulsion frequency and the larger scale of the fluvial channel belts.

7.5. Tectonic control

The overall parallel disposition of siltstone and mudstone strata in the study stratigraphic interval indicates that the local relief was relatively flat. Other indirect evidences of scarce tectonic activity during

the deposition of the study stratigraphic interval is the lack of incised valleys, terraces or other features associated to degradational landscape, indicating that the system was dominantly aggradational.

7.6. Base-level control

Legarreta et al. (1993) related base-level shifts using the vertical variation in the proportion of channel belts and floodplain fines, defining "foresteeping", backsteeping" and "aggradational" system tracts. The sequence stratigraphy nomenclature proposed by Martinsen et al. (1999) is the one that best applies to this study, where the fluvial succession of the Cerro Ballena can be characterized by a single, well-defined sequence with two systems tracts. Sediments within the Section A can be interpreted as a high-accommodation system tract due to the low interconnectivity of the channel belts, with stacking density of 12%. Channel belts of Section A are narrower that those of Section B, and can be associated to higher aggradation rate of floodplain materials in relation to avulsion frequency. On the other hand, deposits within Section B are considered a low-accommodation system tract characterized by elevated connectivity of channel belts. Averaged stacking density of Section B is 32%, reflecting reduced aggradation floodplain rate in relation to lateral shift of the channel belts on the floodplain. Although the model could of Martinsen et al. (1999) can be applied to the study interval, sequence models associated to base-level variation requires the presence of large incisional relief in the base of amalgamated channel complexes and development of mature paleosols in interfluves as evidence of significative base level shifts (Hampson et al., 2005), and development of sequence boundaries. As neither of these features have been identified in the study exposures, we can not demonstrate base level control on the alluvial organization. Alternatively, the observed differences in the stacking density between sections A and B can be explained by changes in other forcing factors, as it was explained above.

8. Concluding remarks

1) Facies analysis and alluvial architecture in the Upper Cretaceous Bajo Barreal Formation along the Cerro Ballena anticline, central Patagonia, show the vertical changes in stacking density and scale of palaeorivers during a climatic shift toward more humid and wetter conditions throughout the studied succession. The fluvial strata show two main lithological sections. The lowermost Section A consists of grey siliciclastic mudstones and siltstones with isolated channel belts of small size, whereas the overlying Section B consists of tuffaceous mudstones and larger-scale channel belts with higher interconnectivity.
2) Seventeen sedimentary facies and 12 architectural elements provide information on the organization of channels and overbank deposits. Five architectural styles for channel-belts, and two channel-belt-complex styles demonstrate the presence of a complex fluvial architecture. A multichannel fluvial system (largely anabranching, locally anastomosed) is suggested by the large number of coeval channels of varying dimensions and architectural style, with lateral variation in the internal architecture and grain size of channel fills, and the presence of tabular sandstones interpreted as crevasse splays. Although some sandstone bodies have well developed lateral accretion surfaces, most of the channels migrated by incisional avulsion.
3) Average palaeocurrent values in sandstone facies of 218 fluvial channels indicate variable SSW and SSE oriented palaeocurrent direction (Az. 187°; n = 3777) and indicate the presence of a depocenter located south of the Deseado river.
4) Increase in stacking density from Sections A to Section B is associated to a climatic shift upward in the sedimentary succession, a trend identified using palaeohydrological parameters. Rivers of Section B were deeper, wider and they carried larger discharges than fluvial channels of Section A. Increase of the avulsion frequency associated to increased sediment supply of rivers of Section B is the probable explanation of the increase in interconnectivity, which has even compensated the increase of floodplain aggradation rate associated to delivery of ash particles onto the drainage network.

Acknowledgments

We would like to thank SINOPEC ARGENTINA E&P for the permission to publish the results. The authors are indebted to landowners of estancia Cañadon Vasco (family Bain) for access to outcrops. We also express our gratitude to A.M. Umazano, C.M.S. Scherer and an anonymus reviewer for their constructive remarks as journal referees. This research was partially supported by the Agencia Nacional de Promoción Científica y Tecnológica (PICT 2012-1369).

Appendix A. Supplementary data

Supplementary data related to this article can be found at http://dx.doi.org/10.1016/j.jsames.2018.05.007.

References

Alexander, J., Fielding, C.R., 1997. Gravel antidunes in the tropical Burdekin river, Queensland, Australia. Sedimentology 44, 327–337.
Allard, J.O., Paredes, J.M., Foix, N., Giacosa, R.E., 2015. Conexión cretácica entre las cuencas del Golfo San Jorge y Cañadón Asfalto (Patagonia): paleogeografía, implicancias tectonoestratigráficas y su potencial en la exploración de hidrocarburos. Rev. Asoc. Geol. Argent. 72, 21–37.
Allen, J.P., Fielding, C.R., Rygel, M.C., Gibling, M.R., 2013. Deconvolving signals of tectonic and climatic controls from continental basins: and example from the late Paleozoic Cumberland Basin, Atlantic Canada. J. Sediment. Res. 83, 847–872.
Allen, J.P., Fielding, C.R., Gibling, M.R., Rygel, M.C., 2014. Recognizing products of palaeoclimate fluctuations in the fluvial stratigraphic record: an example from the Pennsylvanian to lower permian of Cape Breton Island, Nova Scotia. Sedimentology 61, 1332–1381.
Allen, J.R.L., 1965. Fining upward cycles in alluvial successions. Geol. J. 4, 229–246.
Allen, J.R.L., 1970. Physical Processes of Sedimentation. Allen and Unwin, London, pp. 248.
Archangelsky, S., Bellosi, E., Jalfin, G.A., Perrot, C., 1994. Palynology and alluvial facies from mid-Cretaceous of Patagonia, subsurface of san Jorge Basin, Argentina. Cretac. Res. 15, 127–142.
Ashworth, P.J., Sambrook Smith, G.H., Best, J.L., Bridge, J.S., Lane, S.N., Lunt, I.A., Reesink, A.J.H., Simpson, C.J., Thomas, R.E., 2011. Evolution and sedimentology of a sandy braided channel fill and its differentiation from compound bar deposits. Sedimentology 58, 1860–1883.
Aslan, A., Blum, M.D., 1999. Contrasting styles of Holocene avulsion, Texas Gulf coastal plain. In: In: Smith, N.D., Rogers, J.J. (Eds.), Current Research in Fluvial Sedimentology, vol. 28. International Association of Sedimentologists, Special Publication, pp. 93–209.
Barcat, C., Cortiñas, J., Nevistic, V., Zucchi, H., 1989. Cuenca Golfo san Jorge. In: Chebli, G., Spalletti, L.A. (Eds.), Cuencas Sedimentarias Argentinas. Serie Correlación Geológica, vol. 6. Universidad Nacional de Tucumán, pp. 319–345.
Blair, T.C., McPherson, J.G., 1994. Alluvial fans and their natural distinction from rivers based on morphology, hydraulic processes, sedimentary processes, and facies assemblages. J. Sediment. Res. 64, 450–489.
Bridge, J.S., 1977. Flow, bed topography, grain size and sedimentary structure in open channel bends: a three-dimensional model. Earth Surf. Process. 2, 401–416.
Bridge, J.S., 1993. The interaction between channel geometry, water flow, sediment transport and deposition in braided rivers. In: In: Best, J.L., Bristow, C.S. (Eds.), Braided Rivers, vol. 75. Geological Society of London, Special Publication, pp. 13–71.
Bridge, J.S., 2003. Rivers and Floodplains: Forms, Processes and Sedimentary Record. Blackwell, Oxford, U.K., pp. 491.
Bridge, J.S., Leeder, M.R., 1979. A simulation model of alluvial stratigraphy. Sedimentology 26, 617–644.
Bridge, J.S., Mackey, S.D., 1993. A theoretical study of fluvial sandstone body dimensions. In: In: Flint, S.S., Bryant, I.D. (Eds.), Geological Modeling of Hydrocarbon Reservoirs, vol. 15. International Association of Sedimentologists, Special Publication, pp. 213–236.
Bridge, J.S., Tye, R.S., 2000. Interpreting the dimensions of ancient fluvial channel bars, channels, and channel belts from wireline-logs and cores. AAPG (Am. Assoc. Pet. Geol.) Bull. 84, 1205–1228.
Bridge, J.S., Jalfin, G.A., Georgieff, S.M., 2000. Geometry, lithofacies, and spatial distribution of Cretaceous fluvial sandstone bodies, San Jorge Basin, Argentina: outcrops analog for the hydrocarbon-bearing Chubut Group. J. Sediment. Res. 70, 319–337.
Bristow, C.S., 1993. Sedimentary structures exposed in bar tops in the Brahmaputra River, Bangladesh. In: In: Best, J.L., Bristow, C.S. (Eds.), Braided Rivers, vol. 75. Geological Society of London, Special Publication, pp. 277–289.
Brown, L.F., Barcat, C., Fisher, L.W., Nevistic, A., 1982. Seismic stratigraphic and

depositional systems analysis: new exploration approaches applied to the Gulf of San Jorge Basin, Argentina. In: 1st Congreso Nacional de Hidrocarburos, Petróleo y Gas, pp. 127–156 Mar del Plata.
Casal, G.A., Martínez, R.D., Luna, M., Sciutto, J.C., Lamanna, M.C., 2007. Aeolosaurus colhuehuapensis sp. nov. (Sauropoda, Titanosauria) de la Formación Bajo Barreal, Cretácico Superior de Argentina. Rev. Bras. Palaontol. 10, 53–62.
Casal, G.A., Allard, J.O., Foix, N., 2015. Análisis estratigráfico y paleontológico del Cretácico Superior en la Cuenca del Golfo San Jorge: nueva unidad litoestratigráfica para el Grupo Chubut. Rev. Asoc. Geol. Argent. 72, 81–99.
Catuneanu, O., 2006. Principles of Sequence Stratigraphy. Elsevier, Oxford, pp. 375.
Chelotti, L.A., 1997. Evolución tectónica de la Cuenca del Golfo San Jorge en el Cretácico y Terciario: algunas observaciones desde la interpretación sísmica. Bol. Inf. Pet. 49, 63–82.
Clavijo, R., 1986. Estratigrafía del cretácico inferior en el sector Occidental de la Cuenca Golfo San Jorge. Bol. Inf. Pet. 9, 15–32.
Cowan, E.J., 1991. The large-scale architecture of the fluvial Westwater Canyon Member, Morrison formation (Jurassic), san juan basin, New Mexico. In: In: Miall, A.D., Tyler, N. (Eds.), The Three-Dimensional Facies Architecture of Terrigenous Clastic Sediments, and its Implications for Hydrocarbon Discovery and Recovery: SEPM Concepts in Sedimentology and Paleontology, vol. 3. pp. 80–93.
Di Benedetto, L., Georgieff, S.M., Potas, G., 2006. Stratigraphic correlation and sedimentary analogs: Ballena Hill outcrops and Cañadón Vasco oil field, southern flank of san Jorge Basin, Argentina. In: Simposio Bolivariano de Hidrocarburos, pp. 12 Cartagena de Indias, Colombia.
El-Mowafy, H.Z., Marfurt, K.J., 2016. Quantitative seismic geomorphology of the middle Frio fluvial system, south Texas, United States. AAPG (Am. Assoc. Pet. Geol.) Bull. 100, 537–564.
Ethridge, F.G., Schumm, S.A., 2007. Fluvial seismic geomorphology: a view from the surface. In: In: Davies, R.J., Posamentier, H.W., Wood, L.J., Cartwright, J.A. (Eds.), Seismic Geomorphology: Applications to Hydrocarbon Exploration and Production, vol. 277. Geological Society, London, Special Publications, pp. 205–222.
Fabuel-Perez, I., Redfern, J., Hodgetts, D., 2009. Sedimentology o fan intra-montane rift-controlled fluvial dominated succession: the upper Triassic Oukaimeden sandstone formation, central high Atlasa, Morocco. Sediment. Geol. 218, 103–140.
Feruglio, E., 1949. Descripción Geológica de la Patagonia. Yacimientos Petrolíferos Fiscales, vol. 1. pp. 334 Buenos Aires.
Fielding, C.R., 1986. Fluvial channel and overbank deposits from the Westphalian of the Durham coalfield, NE England. Sedimentology 33, 119–140.
Fielding, C.R., 2006. Upper flow regime sheets, lenses and scour fills: extending the range of architectural elements for fluvial sediment bodies. Sediment. Geol. 190, 227–240.
Figari, E.G., Hechem, J.J., Homovc, J.F., 1990. Arquitectura depositacional de las “Areniscas Verdes” de la Formación Bajo Barreal, provincia del Chubut, Argentina. In: 3rd Reunión Argentina de Sedimentología, vol. 1. pp. 130–138 San Juan.
Figari, E.G., Cid de la Paz, M.S., Laffitte, G., 1996. Neocomian half grabens in the western San Jorge Basin, Argentina: petroleum systems, origin and tectonic inversion. AAPG (Am. Assoc. Pet. Geol.) Bull. 80, 1289–1290.
Figari, E.G., Courtade, S.F., Calegari, R., Arroyo, H., Constantini, L., 1998. Estructura y estratigrafía del Cerro Ballena, Faja Plegada meridional de la Cuenca del Golfo San Jorge. In: 10th Congreso Latinoamericano de Geología and 6th Congreso Nacional de Geología Económica, vol. 1. pp. 18–23 Buenos Aires.
Figari, E., Stelkov, E.E., Laffitte, G., Cid de la Paz, M., Courtade, S., Celaya, J., Vottero, A., Lafourcade, P., Martinez, R., Villar, H., 1999. Los sistemas petroleros de la Cuenca del Golfo San Jorge: Síntesis estructural, estratigráfica y geoquímica. In: 4th Congreso de Exploración y Desarrollo de Hidrocarburospp. 197–237 Buenos Aires.
Fisher, J.A., Nichols, G.J., Waltham, D.A., 2007. Unconfined flow deposits in distal sectors of fluvial distributary systems: examples from the Miocene Luna and Huesca Systems, northern Spain. Sediment. Geol. 195, 55–73.
Fitzgerald, M.G., Mitchum, R.M., Uliana, M.A., Biddle, K.T., 1990. Evolution of the san Jorge Basin, Argentina. AAPG (Am. Assoc. Pet. Geol.) Bull. 74, 879–920.
Foix, N., Paredes, J.M., Giacosa, R.E., 2008. Paleo-earthquakes in passive-margin settings, an example from the Paleocene of the Golfo san Jorge Basin, Argentina. Sediment. Geol. 205, 67–78.
Friend, P.F., 1983. Toward the field classification of alluvial architecture and sequence. In: In: Collinson, J.D., Lewin, J. (Eds.), Modern and Ancient Fluvial Systems, vol. 6. International Association of Sedimentologists, Special Publication, pp. 345–354.
Ghinassi, M., Iepi, A., Aldinucci, M., Fustic, M., 2016. Downstream-migrating fluvial point bars in the rock record. Sediment. Geol. 334, 66–96.
Gibling, M.R., 2006. Width and thickness of fluvial channel bodies and valley fills in the geological record: a literature compilation and classification. J. Sediment. Res. 76, 731–770.
Hajek, E.A., Wolinsky, M.A., 2012. Simplified process modeling of river avulsion and alluvial architecture: connecting models and field data. Sediment. Geol. 257, 1–30.
Hampson, G.J., Davies, W., Davies, S.J., Howell, J.A., Adamson, K.R., 2005. Use of spectral gamma-ray data to refine subsurface fluvial stratigraphy: late Cretaceous strata in the Book Cliffs, Utah, USA. J. Geol. Soc. Lond. 162, 603–621.
Hampson, G.J., Jewell, T.O., Ifran, N., Gani, M.R., Bracken, B., 2013. Modest change in fluvial style with varying accommodation in regressive alluvial-to-coastal plain wedge: Upper Cretaceous Blackhawk Formation, Wasatch Plateau, central Utah, U.S.A. J. Sediment. Res. 83, 145–169.
Hechem, J.J., 1994. Modelo predictivo de reservorios en un sistema fluvial efímero del Chubutiano de la cuenca del Golfo San Jorge, Argentina. Rev. Asoc. Argent. Sedimentol. 1, 3–14.
Hechem, J.J., 1997. Arquitectura y paleodrenaje del sistema fluvial efímero de la Formación Bajo Barreal, cuenca del Golfo San Jorge, Argentina. In: 1st Congreso Latinoamericano de Sedimentología, vol. 1. pp. 315–323 Isla Margarita (Venezuela).
Hechem, J.J., Strelkov, E.E., 2002. Secuencia sedimentaria mesozoica del Golfo San Jorge. In: In: Haller, J.M. (Ed.), Geología y Recursos Naturales de Santa Cruz. Relatorio del 15th Congreso Geológico Argentino, vol. 1. pp. 129–147 Buenos Aires.
Hechem, J.J., Homovc, J.F., Figari, E.G., 1990. Estratigrafía del Chubutiano (Cretácico) en la Sierra de San Bernardo, cuenca del Golfo San Jorge, Argentina. In: 11th Congreso Geológico Argentino, vol. 3. pp. 173–176 San Juan.
Heller, P.L., Paola, C., 1996. Downstream changes in alluvial architecture: an exploration of controls on channel-stacking patterns. J. Sediment. Res. 66, 297–306.
Heller, P.L., Ratigan, D., Trampush, S., Noda, A., McElroy, B., Drever, J., Huzurbazar, S., 2015. Origins of bimodal stratigraphy in fluvial deposits: an example from the Morrison Formation (Upper Jurassic), western U.S.A. J. Sediment. Res. 85, 1466–1477.
Hickson, T.A., Sheets, B.A., Paola, C., Kelberer, M., 2005. Experimental test of tectonic controls on three-dimensional alluvial facies architecture. J. Sediment. Res. 75, 710–722.
Jo, H.R., 2003. Depositional environments, architecture, and controls of Early Cretaceous non-marine successions in the north-eastern part of Kyongsang Basin. Sediment. Geol. 161, 269–294.
Jones, C.M., 1977. Effects of varying discharge regimes on bed-form sedimentary structures in modern rivers. Geology 5, 567–570.
Jones, H.J., Hajek, E.A., 2007. Characterising avulsion stratigraphy in ancient alluvial deposits. Sediment. Geol. 202, 124–137.
Jorgensen, P.J., Fielding, C.R., 1996. Facies architecture of alluvial floodbasin deposits: three-dimensional data from the Upper Triassic Callide coal measures of east-central Queensland, Australia. Sedimentology 43, 479–495.
Karssenberg, D., Tornqvist, T.E., Bridge, J.S., 2001. Conditioning a process-based model of sedimentary architecture to well data. J. Sediment. Res. 71, 868–879.
Kataoka, K., 2009. Impacts of explosive volcanism on distal alluvial sedimentation: Examples from the Pliocene-Holocene volcaniclastic successions of Japan. Sediment. Geol. 220, 306–317.
Keogh, K.J., Leary, S., Martinius, A.W., Scott, A.S.J., Riordan, S., Viste, I., Gowland, S., Taylor, A.M., Howell, J., 2014. Data capture for multiscale modelling of the Lourinhã Formation, Lusitanian Basin, Portugal: an outcrop analogue for the Statfjord Group, Norwegian North Sea. In: In: Martinius, A.W., Howell, J.A., Good, T.R. (Eds.), Sediment-Body Geometry and Heterogeneity: Analogue Studies for Modelling the Subsurface, vol. 387. Geological Society of London, Special Publications, pp. 27–56.
Kraus, M.J., 1996. Avulsion deposits in lower Eocene alluvial rocks, Bighorn Basin. J. Sediment. Res. 66, 354–366.
Labourdette, R., 2011. Stratigraphy and static connectivity of braided fluvial deposits of the lower Escanilla Formation, south central Pyrenees, Spain. AAPG (Am. Assoc. Pet. Geol.) Bull. 95, 585–617.
Leclair, S.F., 2002. Preservation of cross strata due to migration of subaqueous dunes: an experimental investigation. Sedimentology 49, 1157–1180.
Leclair, S.F., Bridge, J.S., 2001. Quantitative interpretation of sedimentary structures formed by river dunes. J. Sediment. Res. 71, 713–716.
Leeder, M.R., 1973. Fluviatile fining-upwards cycles and the magnitude of paleochannels. Geol. Mag. 110, 265–276.
Legarreta, L., Uliana, M., Larotonda, C.A., Meconi, G.R., 1993. Approaches to nonmarine sequence stratigraphy - theoretical models and examples from Argentine basins. In: In: Eschard, R., Doliez, B. (Eds.), Subsurface Reservoir Characterization from Outcrop Observations. Collection Colloques et Séminaires, vol. 51. Editions Technip, Paris, pp. 125–145.
Leopold, L.B., Wolman, G.M., Miller, J.P., 1964. Fluvial Processes in River Geomorphology. Freeman, San Francisco, pp. 522.
Lesta, P., 1968. Estratigrafía de la Cuenca del Golfo San Jorge. In: 3rd Jornadas Geológicas Argentinas, vol. 1. pp. 251–280 Buenos Aires.
Lesta, P., Ferello, R., 1972. Región Extraandina del Chubut y norte de Santa Cruz. In: In: Leanza, A. (Ed.), Geología Regional Argentina Academia Nacional de Ciencias, Córdoba, pp. 601–654.
Lewin, J., Ashworth, P.J., 2014. Defining large river channel patterns: alluvial exchange and plurality. Geomorphology 215, 83–98.
Makaske, B., 2001. Anastomosing rivers: a review of their classification, origin and sedimentary products. Earth Sci. Rev. 53, 149–196.
Makaske, B., Berendsen, J.A., van Ree, M.H.M., 2007. Middle Holocene avulsion-belt deposits in the Central Rhine-Meuse delta, The Netherlands. J. Sediment. Res. 77, 110–123.
Makaske, B., Lavooi, E., De Haas, T., Kleinhans, M., Smith, D.G., 2017. Upstream control of river anastomosing by sediment overloading, upper Columbia river, British Columbia, Canada. Sedimentology 64, 1488–1510.
Martínez, R.D., Lamanna, M.C., Novas, F.E., Ridgely, R.C., Casal, G.A., Martínez, J.E., Vita, J.R., Witmer, L.M., 2016. A basal lithostrotian titanosaur (Dinosauria: Sauropoda) with a complete skull: implications for the evolution and paleobiology of Titanosauria. PLoS One 11, e0151661. http://dx.doi.org/10.1371/journal.pone.0151661.
Martinsen, O., Ryseth, A., Hansen, W.H., Fleshe, H., Torkildsen, G., Idil, S., 1999. Stratigraphic base level and fluvial architecture: Ercson Sandstone (Campanian), Rock Springs Uplift, SW Wyoming, USA. Sedimentology 46, 235–259.
Melvin, J., 1987. Fluvio-paludal deposits in the lower Kekiktuk Formation (Mississippian), Endicott Field, northeast Alaska. In: In: Ethridge, F.G., Flores, R.M., Harvey, M.D. (Eds.), Recent Developments in Fluvial Sedimentology: 3rd International Fluvial Sedimentology Conference, vol. 39. SEPM, Special Publication, pp. 343–352.
Miall, A.D., 1985. Architectural-element analysis: a new method of facies analysis applied to fluvial deposits. Earth Sci. Rev. 22, 261–308.
Miall, A.D., 1996. The Geology of Fluvial Deposits. Springer, Berlín, pp. 582.
Miall, A.D., 2014. Fluvial Depositional Systems. Springer, Switzerland, pp. 316.
Mohrig, D., Heller, P.L., Paola, C., Lyons, W.J., 2000. Interpreting avulsion process from

ancient alluvial sequences: Guadalupe-Matarranya (Northern Spain) and Wasatch Formation (Western Colorado). Geol. Soc. Am. Bull. 112, 1787–1803.
Nanson, G.C., Knighton, A.D., 1996. Anabranching rivers-their cause, character and classification. Earth Surf. Process. Landforms 21, 217–239.
Navarrete, C.R., Gianni, G.M., Folguera, A., 2015. Tectonic inversion events in the western San Jorge Gulf Basin from seismic, borehole and field data. J. S. Am. Earth Sci. 64, 486–497.
Nemec, W., Steel, R.J., 1984. Alluvial and coastal conglomerates: their significant features and some comments on gravelly massflow deposits. In: In: Koster, E.H., Steel, R.J. (Eds.), Sedimentology of Gravels and Conglomerates, vol. 10. Canadian Society of Petroleum Geologists Memoir, pp. 1–31.
North, C.P., Taylor, K.S., 1996. Ephemeral-fluvial deposits: integrated outcrop and simulation studies reveal complexity. AAPG (Am. Assoc. Pet. Geol.) Bull. 80, 811–830.
North, C.P., Nanson, G.C., Fagan, S.D., 2007. Recognition of the sedimentary architecture of dryland anabranching (anastomosing) rivers. J. Sediment. Res. 77, 925–938.
Osterkamp, W.R., Hedman, E.R., 1982. Perennial streamflow characteristics related to channel geometry and sediment in the Missouri River basin. USGS Professional Paper 1242, 1–37.
Ouchi, S., 1985. Response of alluvial rivers to slow active tectonic movement. Geol. Soc. Am. Bull. 96, 504–515.
Paredes, J.M., Foix, N., Colombo Piñol, F., Nillni, A., Allard, J.O., Marquillas, R.A., 2007. Volcanic and climatic controls on fluvial style in a high-energy system: The Lower Cretaceous Matasiete Formation, Golfo San Jorge Basin, Argentina. Sediment. Geol. 202, 96–123.
Paredes, J.M., Foix, N., Allard, J.O., Colombo, F., Tunik, M.A., 2015. Alluvial architecture of reworked pyroclastic deposits in peri-volcanic basins: Castillo Formation (Albian) of the Golfo San Jorge Basin, Argentina. Rev. Asoc. Geol. Argent. 72, 42–62.
Paredes, J.M., Foix, N., Allard, J.O., 2016. Sedimentology and alluvial architecture of the Bajo Barreal Formation (Upper Cretaceous) in the Golfo San Jorge Basin: outcrop analogues of the richest oil-bearing fluvial succession in Argentina. Mar. Petrol. Geol. 72, 317–335.
Paredes, J.M., Aguiar, M., Ansa, A., Giordano, S.R., Ledesma, M., Tejada, S., 2018. Inherited discontinuities and fault kinematics of a multiphase, non-colinear extensional setting: Subsurface observations from the South Flank of the Golfo San Jorge Basin, Patagonia. J. S. Am. Earth Sci. 81, 87–107.
Peroni, G., Hegedus, A., Cerdan, J., Legarreta, L., Uliana, M., Laffite, G., 1995. Hydrocarbon accumulation in an inverted segment of the Andean Foreland: San Bernardo Belt, Central Patagonia. In: In: Tankard, A., Suarez, R., Welsink, H. (Eds.), Petroleum Basins of South America, vol. 62. American Association of Petroleum Geologists Memoir, Tulsa, pp. 403–419.
Posamentier, H.W., Davies, R.J., Cartwright, J.A., Wood, L., 2007. Seismic geomorphology - an overview. In: In: Davies, R.J., Posamentier, H.W., Wood, L.J., Cartwright, J.A. (Eds.), Seismic Geomorphology: Applications to Hydrocarbon Exploration and Production, vol. 277. Geological Society of London, Special Publications, pp. 1–14.
Potter, P.E., 1967. Sand bodies and sedimentary environments: a review. AAPG (Am. Assoc. Pet. Geol.) Bull. 51, 337–365.
Pranter, M.J., Sommer, M.K., 2011. Static connectivity of fluvial sandstones in a lower coastal-plain setting: An example from the Upper Cretaceous lower Williams Fork Formation, Piceance Basin, Colorado. AAPG (Am. Assoc. Pet. Geol.) Bull. 95, 899–923.
Pranter, M.J., Hewlett, A.C., Cole, R.D., Wang, H., Gilman, J., 2014. Fluvial architecture and connectivity of the Williams Fork Formation: use of outcrop analogues for stratigraphic characterization and reservoir modelling. In: In: Martinius, A.W., Howell, J.A., Good, T.R. (Eds.), Sediment-body Geometry and Heterogeneity: Analogue Studies for Modelling the Subsurface, vol. 387. Geological Society of London, Special Publications, pp. 57–83.
Ramsay, J.G., 1961. The effects of folding upon the orientation of sedimentary structures. J. Geol. 69, 84–100.
Reesink, A.J.H., Bridge, J.S., 2007. Influence of superimposed bedforms and flow unsteadiness on formation of cross strata in dunes and unit bars. Sediment. Geol. 202, 281–296.
Reesink, A.J.H., Bridge, J.S., 2009. Influence of bedform superimposition and flow unsteadiness on the formation of cross strata in dunes and unit bars – Part 2, further experiments. Sediment. Geol. 222, 274–300.
Reijenstein, H.M., Posamentier, H.W., Bhattacharya, J.P., 2011. Seismic geomorphology and high-resolution seismic stratigraphy of inner-shelf, fluvial, estuarine, deltaic and marine sequences, Gulf of Thailand. AAPG (Am. Assoc. Pet. Geol.) Bull. 95, 1959–1990.
Rittersbacher, A., Buckley, S.J., Howell, J.A., Hampson, G.J., Vallet, J., 2014. Helicopter-based laser scanning: a method for quantitative analysis of large-scale sedimentary architecture. In: In: Martinius, A.W., Howell, J.A., Good, T.R. (Eds.), Sediment-body Geometry and Heterogeneity: Analogue Studies for Modelling the Subsurface, vol. 387. Geological Society of London, Special Publications, pp. 185–202.
Rodriguez, J.F.R., 1993. La depositación de las areniscas verdes (Formación Bajo Barreal-Cretácico Tardío) y sus implicancias tafonómicas. In: 12th Congreso Geológico Argentino and 2nd Congreso de Exploración de Hidrocarburos, pp. 194–199 Mendoza.
Rodriguez, J.F.R., Littke, R., 2001. Petroleum generation and accumulation in the Golfo San Jorge Basin, Argentina: a basin modeling study. Mar. Petrol. Geol. 18, 995–1028.
Sambrook Smith, G.H., Best, J.L., Leroy, J.Z., Orfeo, O., 2016. The alluvial architecture of a suspended sediment dominated meandering river: the Río Bermejo, Argentina. Sedimentology 63, 1187–1208.
Schumm, S.A., 1968. Speculations concerning palaeohydrologic controls of terrestrial sedimentation. Geol. Soc. Am. Bull. 79, 1573–1588.
Schumm, S.A., 1969. River metamorphosis. Journal of the Hydraulics Division. Am. Soc. Civ. Eng. 95, 255–273.
Schumm, S.A., 1985. Patterns of alluvial rivers. Annu. Rev. Earth Planet Sci. 13, 5–27.
Schumm, S.A., 1993. River response to baselevel change: implications for sequence stratigraphy. J. Geol. 101, 279–294.
Sciutto, J.C., 1981. Geología del Codo del Río Senguerr, Chubut, Argentina. In: 8th Congreso Geológico Argentino, vol. 3. pp. 203–219 San Luis.
Secretaría de Energía, 2016. Informe estadístico anual 2016 del sector energético. Ministerio de Energía y Minería. Secretaría de Planeamiento Energético Estratégico, pp. 40.
Shanley, K.W., McCabe, P.J., 1994. Perspectives on the sequence stratigraphy of continental strata. AAPG (Am. Assoc. Pet. Geol.) Bull. 78, 544–568.
Shultz, A.W., 1984. Subaerial debris-flow deposition in the Upper Paleozoic Cutler Formation, Western Colorado. J. Sediment. Petrol. 54, 749–772.
Slingerland, R.L., Smith, N.D., 2004. River avulsions and their deposits. Annu. Rev. Earth Planet Sci. 32, 257–285.
Smith, G.A., 1986. Coarse-grained nonmarine volcaniclastic sediment: Terminology and depositional process. Geol. Soc. Am. Bull. 97, 1–10.
Smith, G.A., Lowe, D.R., 1991. Lahars: volcano-hydrologic events and deposition in the debris flow-hyperconcentrated flow continuum. In: In: Fisher, R.V., Smith, G.A. (Eds.), Sedimentation in Volcanic Settings, vol. 45. Society for Sedimentary Geology Special Publication, Tulsa, pp. 59–70.
Smith, N.D., Cross, T.A., Dufficy, J.P., Clough, S.R., 1989. Anatomy of an avulsion. Sedimentology 36, 1–23.
Sohn, Y.K., Rhee, C.W., Kim, B.C., 1999. Debris flow and hyperconcentrated flood-flow deposits in an alluvial fan, northwestern part of the Cretaceous Yongdong basin, central Korea. J. Geol. 107, 111–132.
Stouthamer, E., Berendsen, H.J.A., 2001. Avulsion frequency, avulsion duration, and interavulsion period of Holocene channel belts in the Rhine-Meuse Delta, the Netherlands. J. Sediment. Res. 71, 589–598.
Stouthamer, E., Berendsen, H.J.A., 2007. Avulsion: the relative roles of autogenic and allogenic processes. Sediment. Geol. 198, 309–325.
Thouret, J.-C., Lavigne, F., 2000. Lahars: ocurrence, deposits and behaviour of volcano-hydrologic flows. In: Leyrit, H., Montenat, C. (Eds.), Volcaniclastic Rocks, from Magmas to Sediments. Gordon & Beach Science Publishers, pp. 151–174.
Uliana, M.A., Biddle, K.T., Cerdán, J., 1989. Mesozoic extension and the formation of Argentine sedimentary basins. In: In: Tankard, A.J., Balkwill, H.R. (Eds.), Extensional Deformation and Stratigraphy of the North Atlantic Margins, vol. 46. American Association of Petroleum Geologists Memoir, Tulsa, pp. 599–614.
Umazano, A.M., Bellosi, E.S., Visconti, G., Melchor, R.N., 2008. Mechanism of aggradation in fluvial systems influenced by explosive volcanism: an example from the Upper Cretaceous Bajo Barreal Formation, San Jorge Basin, Argentina. Sediment. Geol. 203, 213–228.
Umazano, A.M., Bellosi, E.S., Visconti, G., Jalfin, G.A., Melchor, R.N., 2009. Sedimentary record of a Late Cretaceous volcanic arc in Central Patagonia: petrography, geochemistry and provenance of fluvial volcaniclastic deposits of the Bajo Barreal Formation, San Jorge Basin, Argentina. Cretac. Res. 30, 749–766.
Umazano, A.M., Bellosi, E.S., Visconti, G., Melchor, R.N., 2012. Detecting allocyclic signals in volcaniclastic fluvial successions: Facies, architecture and stacking pattern from the Cretaceous of central Patagonia, Argentina. J. S. Am. Earth Sci. 40, 94–115.
Van der Neut, M., Eriksson, P.G., 1999. Palaeohydrological parameters of a Proterozoic braided fluvial system (Wilgerivier Formation, Waterberg Group, South Africa) compared with a Phanerozoic example. Special Publ. Int. Assoc. Sedimentol. 28, 381–392.
Williams, G.P., 1978. Bank-full discharge of rivers. Water Resour. Res. 14, 1141–1154.
Wilson, A., Flint, S., Payenberg, T., Tohver, E., Lanci, L., 2014. Architectural styles and sedimentology of the fluvial Lower Beaufort Group, Karro Basin, South Africa. J. Sediment. Res. 84, 326–348.